

Review

# A Comprehensive Review of Thermal Management Challenges and Safety Considerations in Lithium-Ion Batteries for Electric Vehicles

Ali Alawi , Ahmed Saeed , Mostafa H. Sharqawy \*  and Mohammad Al Janaideh

College of Engineering, University of Guelph, Guelph, ON N1G 2W1, Canada

\* Correspondence: melsharq@uoguelph.ca; Tel.: +1-(519)-824-4120 (ext. 58973)

## Abstract

The transition to electric vehicles (EVs) is accelerating due to global efforts to reduce greenhouse gas emissions and reliance on fossil fuels. Lithium-ion batteries (LIBs) are the predominant energy storage solution in EVs, offering high energy density, efficiency, and long lifespan. However, their adoption is overly involved with critical safety concerns, including thermal runaway and overheating. This review systematically focuses on the critical role of battery thermal management systems (BTMSs), such as active, passive, and hybrid cooling systems, in maintaining LIBs within their optimal operating temperature range, ensuring temperature homogeneity, safety, and efficiency. Additionally, the study explores the impact of integrating artificial intelligence (AI) and machine learning (ML) into BTMS on thermal performance prediction and energy-efficient cooling, focusing on optimizing the operating parameters of cooling systems. This review provides insights into enhancing LIB safety and performance for widespread EV adoption by addressing these challenges.

**Keywords:** electric vehicles (EVs); lithium-ion batteries (LIBs); battery thermal management system (BTMS); thermal runaway; fault diagnosis; battery aging; high-temperature effects; low-temperature effects; battery safety; energy storage; battery degradation; sensor faults; battery performance; electrolyte innovation; green transportation



Academic Editors: Xianglin Li and Ottorino Veneri

Received: 16 April 2025

Revised: 14 July 2025

Accepted: 16 July 2025

Published: 19 July 2025

**Citation:** Alawi, A.; Saeed, A.; Sharqawy, M.H.; Al Janaideh, M. A Comprehensive Review of Thermal Management Challenges and Safety Considerations in Lithium-Ion Batteries for Electric Vehicles. *Batteries* **2025**, *11*, 275. <https://doi.org/10.3390/batteries11070275>

**Copyright:** © 2025 by the authors. Licensee MDPI, Basel, Switzerland. This article is an open access article distributed under the terms and conditions of the Creative Commons Attribution (CC BY) license (<https://creativecommons.org/licenses/by/4.0/>).

## 1. Introduction

The transportation sector's reliance on internal combustion engines (ICEs) has significantly contributed to global CO<sub>2</sub> emissions, prompting a shift toward cleaner alternatives like electric vehicles (EVs) [1–4]. Among EV power sources, lithium-ion batteries (LIBs) dominate due to their high energy density, long lifespan, and lack of memory effect, ensuring consistent performance regardless of their charge-discharge history [5,6]. However, despite their advantages, widespread EV adoption faces challenges related to battery safety, reliability, and performance degradation, particularly under extreme thermal conditions [7,8]. These safety concerns generally fall into two categories, namely fault diagnosis issues and thermal management faults [9]. Fault diagnosis challenges include battery abuse, sensor malfunctions, and connection issues [10]. Thermal management faults involve inefficient cooling methods, uneven temperature distribution within battery packs, and improperly placed temperature sensors. Consequently, intensive research is directed at mitigating these risks and developing advanced safety measures for batteries in EVs [11,12].

Batteries in real applications are required to operate at an optimum temperature range to ensure the efficiency and safety of the system [13]. High temperatures have

several negative consequences on battery operation, including fading capacity/power and self-discharge [14], which can cause a significant loss of available energy [15]. Thomas et al. [16] performed an accelerated aging experiment to investigate the effect of aging duration and temperature on the functionality of Li-ion cells, and they discovered that a power fade of 55% was achieved over a 20-week storage period at 55 °C. Bandhauer et al. [17] studied different positive electrode materials' capacity and power fading during high-temperature cycling and storage. Researchers discovered that the capacity decreased when the temperature exceeded ~50 °C. A. Saeed et al. [18] studied the calendar aging of 27 NRC18650B cells under real-world summer conditions in Saudi Arabia. The cells were grouped by state of charge (50%, 75%, 100%) and storage conditions (lab at 21 °C, outdoor shade, or sun-exposed aluminum box). Results showed that storage temperature greatly affects battery performance, especially at full charge (100% SoC). The harshest conditions—direct sunlight, full charge, and glass-covered storage—led to a 6% drop in state of health (SoH), a 6.5% rise in internal resistance, and slight declines in coulombic and energy efficiencies (both 2%). Gao et al. [19] studied how aging temperature affects the thermal stability of lithium-ion batteries (LIB). They cycled four sets of commercial LIBs at 25 °C, 60 °C, and 80 °C for 100 cycles and analyzed electrode and separator changes. The study found that solid electrolyte interphase (SEI) layer composition shifts significantly influence TR behavior and electrical performance.

The performance of LIBs is not only a function of high temperatures but can also deteriorate at low temperatures. Low temperature degrades battery performance and limits application in cold locations, such as high-altitude drones [20,21]. Low temperatures affect batteries, including charge acceptance, which refers to the battery's ability to effectively store energy during charging, power capacity reduction, round-trip efficiency, and longevity. Kong et al. [22] studied experimentally the impact of low temperatures on the TR and fire behavior of 18650 LIBs. The results revealed that the onset temperature of TR fell dramatically when the operating temperature lowered from 25 °C to −10 °C. Low-temperature cycling causes safety valve fracture and TR to happen sooner. Smart et al. [23] developed quaternary carbonate-based electrolytes (e.g., 1.0 M LiPF<sub>6</sub> in EC/DEC/DMC/EMC blends) to improve lithium-ion battery performance at extremely low temperatures (down to −40 °C). Testing in prototype DD-size cells demonstrated high energy delivery (95 Wh/kg at −40 °C, C/10 rate) and stable cycling, even at −70 °C under ultra-low discharge rates. The optimized electrolytes enhanced ionic conductivity and electrode kinetics while minimizing lithium plating risks during low-temperature charging. This advancement supports NASA's Mars missions, where batteries must operate in harsh environments.

An efficient battery thermal management system (BTMS) is essential to maintain Li-ion batteries within their optimal 15–35 °C range while limiting temperature variations ( $\Delta T_m < 5$  °C) [24,25]. Integrating AI and machine learning (ML) into BTMS enhances thermal control by predicting real-time thermal behavior and optimizing cooling/heating adjustments. AI algorithms analyze temperature, performance, and environmental data to ensure stable operation under varying conditions. They also enable adaptive thermal management by detecting early TR or performance degradation signs. Neural networks and reinforcement learning optimize energy use, activating cooling only when necessary to reduce power waste. This AI-driven approach improves temperature regulation, extends battery lifespan, and enhances system reliability by preventing overheating and minimizing performance loss. Ultimately, AI-powered BTMS supports safer, more efficient battery applications.

Consequently, this paper aims to present a detailed examination of advances in BTMS for EVs, with particular attention placed on incorporating AI and ML methods. Various

BTMS techniques are carefully investigated to determine their ability to maintain ideal thermal conditions in LIBs. Moreover, the role of AI in BTMS applications adds an intelligent, adaptive layer of control that improves the system's ability to manage temperature more efficiently, ensuring safety, extending battery life, and optimizing energy consumption. Furthermore, this paper will cover known AI methodologies and the limited large-scale commercial implementation of AI-enhanced BTMS, focusing on obstacles such as system complexity, integration costs, and the requirement for significant data for reliable AI modeling. Therefore, this review aims to provide a critical perspective on the future path of BTMS development, highlighting current limitations and AI and ML's significant opportunity to revolutionize thermal management in EVs.

## 2. Battery Thermal Management Systems

LIBs are essential components of modern energy storage systems, with widespread application in portable devices, electric automobiles, and grid energy storage [26]. Several essential characteristics affect their performance, longevity, and safety, including capacity, energy density, power density, cycle life, C-rate, internal resistance, and self-discharge rate [27]. Each characteristic is critical in determining how effectively and reliably a battery performs under varying loads. The capacity to precisely measure and understand these properties is critical for optimizing the design and deployment of LIBs, as well as enhancing their performance and resolving issues such as heat generation, energy losses, and degradation over time [28]. This section systematically discusses these parameters, categorizing them into standard/design parameters and performance parameters while clarifying their significance in advancing the efficiency, safety, and applicability of LIBs. Furthermore, the discussion extends to the thermal modeling of batteries, emphasizing its critical role in predicting heat generation and ensuring optimal thermal management in safeguarding system performance and prolonging operational lifespan.

### 2.1. Design Parameters of LIBs

Several key design parameters govern the performance and efficiency of LIBs in EV applications. These parameters are critical in determining the battery's energy storage capabilities, power delivery, and operational limits [26,27]. These primary design parameters include capacity, energy density, power density, and C-rate. Capacity, which is measured in ampere-hours (Ah), represents the total charge a battery can deliver at a specified current over time [26,27]. For EV applications, the battery system capacities typically range from 20 Ah to 200 Ah, depending on the vehicle size and range requirements [28]. The other parameter is energy density, which indicates the amount of energy stored per unit mass (gravimetric, Wh/kg) or volume (volumetric, Wh/L) [29]. EV batteries typically exhibit gravimetric energy densities of 150–250 Wh/kg and volumetric energy densities of 300–700 Wh/L [28]. On the other hand, power density measures the rate at which energy can be delivered per unit mass (W/kg) or volume (W/L) [30]. The power density range for EV batteries is typically between 300 and 500 W/kg [28]. Lastly, the C-rate defines the charge/discharge current relative to the battery's capacity [31]. The determination of the C-rates under discharging depends on the distance, speed, and load of the EV, while the charging C-rates depend on the capacity of the charging facility or device, whether normal charging or fast charging. Overall, higher C-rates enable rapid charging but generate more heat and accelerate the degradation of the system [32]. Although these parameters are considered standard and set by the battery manufacturers, the temperature fluctuations and inadequate thermal management significantly degrade these parameters [33]. High temperatures accelerate capacity fade, increase internal resistance, reduce power density, and promote thermal runaway [34]. Moreover, low temperatures slow electrochemical reac-

tions, damaging energy and power delivery. Inadequate thermal management exacerbates these effects, creating non-uniform temperature distributions that precipitate accelerated aging and compromise system safety [33]. Consequently, maintaining these design parameters within optimal operational ranges necessitates sophisticated thermal management strategies to ensure battery performance, longevity, and safety in EV applications.

## 2.2. Performance Parameters of LIBs

Several essential design parameters play a pivotal role in shaping the performance of LIBs used in electric vehicles. These factors directly influence the battery's energy storage capacity, power output, and overall operating range. The rest of this section provides a brief review of these key parameters.

### 2.2.1. State of Charge (SoC)

SoC is a crucial LIB performance metric, indicating available capacity relative to full charge (100% = full, 0% = empty) [35]. Precise SoC monitoring is vital for EVs and energy storage systems, enabling battery management systems to prevent damaging overcharge/discharge while optimizing power delivery [36]. Accurate SoC estimation ensures safe operation and meets high-performance application demands by maintaining optimal energy availability throughout discharge cycles.

### 2.2.2. State of Health (SoH)

SoH is a key metric for assessing LIB quality and lifespan, comparing current performance to its original condition [36]. Expressed as a percentage (100% = fresh battery), SoH declines as capacity, power output, and internal resistance degrade over time. Tracking SoH is essential for predicting remaining battery life, optimizing maintenance, and ensuring safety in critical applications like EVs and grid storage.

### 2.2.3. Internal Resistance ( $R_i$ )

Internal resistance is crucial in LIBs, impacting performance, efficiency, and lifespan. It comprises ohmic resistance (from electrolytes/electrodes) and polarization resistance (from electrochemical reactions) [37]. Increased resistance from aging, SEI growth, or electrolyte decomposition causes energy loss as heat, reduced efficiency, and capacity fade, degrading power and longevity [38].

### 2.2.4. Self-Discharge

Self-discharge in LIBs refers to charge loss over time without an external load [39] caused by internal chemical reactions. This reduces available capacity and can harm battery lifespan if prolonged low-charge states damage electrodes or electrolytes. Rates depend on temperature, chemistry, and battery age; higher temperatures worsen self-discharge by accelerating side reactions. Though LIBs self-discharge more slowly than nickel–cadmium or lead–acid batteries, they remain a concern during long storage [40].

### 2.2.5. Coulombic Efficiency (CE)

CE is a key LIB performance metric, measuring the ratio of charge extracted during discharge to charge stored during charging [41]. Expressed as a percentage, it reveals energy losses during cycling and reflects how effectively the battery converts electrical energy into chemical energy and back. Well-functioning LIBs typically exhibit CE above 99%, indicating high charge recovery. Lower CE values result from parasitic reactions, such as electrolyte decomposition, electrode-side reactions, and solid–electrolyte interface (SEI) growth [42]. These inefficiencies contribute to long-term capacity fade and degradation, making CE a vital indicator of battery health and stability over time.

### 2.2.6. Energy Efficiency

Energy efficiency is another key performance measure for LIBs, representing the ratio of energy output during discharge to energy input during charging [43]. It reflects the battery's ability to convert electrical energy into stored chemical energy and back into usable power. High energy efficiency means fewer losses from heat, internal resistance, or side reactions, making it essential for energy-sensitive applications such as electric vehicles and renewable energy storage.

### 2.3. Thermal Model

The heat generated inside the LIB plays a key role in its longevity and efficiency, and this heat is generated inside the cell's core and spreads outward to the battery surface during the charge and discharge process. The heat generation inside the battery is unavoidable because it results from electrical resistance and chemical reactions during charging and discharging cycles. Therefore, the battery must be maintained between 20 °C and 35 °C [44]. On the other hand, the battery's temperature should not be operating at higher and lower temperatures. It has been found that operating LIBs at low temperatures (less than 15 °C) leads to slow electrochemical reactions and increased internal resistance, which will impact the battery's performance, capacity, aging, and power [45]. Furthermore, operating at extreme temperatures exceeding 40 °C can significantly damage the separator material that isolates the cathode and anode.

Elevated temperatures can cause the separator to weaken, melt, or degrade, reducing its effectiveness at preventing direct contact between the two electrodes. This contact between the cathode and the anode can lead to short circuits, where current flows uncontrollably between the anode and cathode. Such short circuits can generate excessive heat, ultimately triggering a phenomenon known as TR. In this scenario, the rapid increase in temperature and pressure within the battery can result in catastrophic failure, including fire, explosion, and the release of hazardous materials such as toxic gases (CO, H<sub>2</sub>, etc.) [46,47]. Therefore, it is crucial to analyze the sources of heat generation. This analysis helps develop an effective thermal management strategy that maintains safe battery temperatures and optimizes efficiency and performance. According to the Bernardi model [48], the heat generation source of the battery during the charging/discharging process is represented in Equation (1) [49]:

$$\dot{Q} = I(V_o - V) - I\left(T \frac{dV_o}{dT}\right) \quad (1)$$

where the first term is the joule heating that results from the internal resistance of the battery ( $I(V_o - V)$ ), the second term is the heat source of the entropy change from the electrochemical reaction of the battery, and represents the reversible term of the heat generation source ( $I\left(T \frac{dV_o}{dT}\right)$ ).  $V_o$  represents the voltage of the open circuit,  $V$  and  $I$  represent the battery's nominal voltage and current, and  $T$  represents the battery's temperature.

The accurate prediction of heat generation within the battery is crucial, as it directly influences the uniformity and consistency of the cell's temperature within the battery pack. A well-designed thermal model can identify hotspots and areas of low thermal resistance, thereby supporting the optimization of battery pack layout and cooling strategies. Enhanced temperature uniformity ensures that all cells operate within their optimal temperature range, reducing the chances of TR. Furthermore, uniform temperature distribution facilitates better performance characteristics across the pack, minimizing performance degradation and maximizing energy efficiency.

### 3. Types of Battery Thermal Management Systems (BTMSs)

The thermal behavior of the EV battery is considered a vital factor influencing its efficiency and lifespan. The battery's performance depends on the temperature and the consistency of the temperature distribution inside the pack. The battery's preferred operating temperature range is 15 °C to 35 °C [25,50], and the temperature difference is less than 5 °C. The increase in the surface temperature of the battery and the hotspot of the temperature inside the battery packs leads to a degradation of battery performance [51]. The heat generation inside the battery comes from the electrochemical reaction and the thermal resistance during the charging and discharging rate [52]. Furthermore, the surrounding condition of the battery, such as extreme weather (hot and cold), influences the performance of the battery [53]. For instance, high temperature increases the self-discharge of the LIBs; thus, the power and capacity of these batteries are reduced accordingly [52,54,55]. Moreover, at low temperatures, the electrolyte reaction inside the cell is slowed down, which results in lithium dendrites on the battery and causes a side reaction [56,57].

Therefore, the BTMS is crucial and considered the heart of EVs. The BTMS has been employed to maintain the battery temperature within the optimal range and to overcome the hotspot regions inside the battery pack. Therefore, the BTMS is key to maintaining the battery under the best operating conditions.

The BTMS is classified into several categories, as illustrated in Figure 1. These categories include internal and external cooling methods, which are further divided into active, passive, and hybrid cooling strategies. Active cooling methods involve systems like air cooling, liquid cooling, and thermoelectric cooling, while passive cooling includes techniques such as phase-change materials and heat pipes. Hybrid cooling combines elements of both active and passive methods. Additionally, the BTMS can utilize various geometries and materials, such as different cathode and anode materials and other battery cell designs.

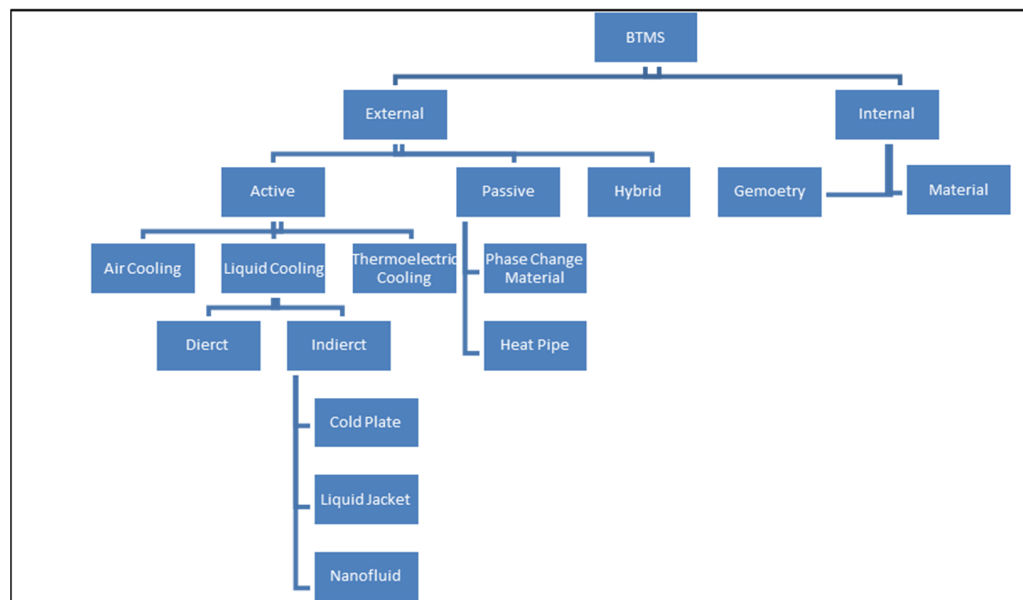


**Figure 1.** Classification of thermal management systems for batteries.

#### 3.1. Active Cooling Technique

The BTMS active cooling essentially depends on the power source, such as a fan, pump, compressor, or condenser, to circulate the coolant [58]. Moreover, it depends on the type of coolant (air, water, oil, nanofluid, etc.) [59]. The active cooling strategies are divided into air, water, and thermoelectric cooling, as shown in Figure 1. For many decades, air has been used for cooling for many reasons, including cost-effectiveness, no leakage risk, and

a simple setup [59]. Liquid active cooling has been recently used extensively because the heat capacity of water is higher than that of air, making active liquid cooling more efficient than air [60,61]. Ultimately, thermoelectric cooling mainly depends on converting electrical energy into the heat difference inside the battery pack, which helps to transfer the heat from the battery surface [62].

### 3.1.1. Air Cooling

Air-based cooling has played a key role in cooling EV batteries for a long time. The reasons for this include the lower installation costs of the cooling system, the absence of leakage risks for the working fluid, and a significantly smaller volume and weight compared to other cooling techniques [63]. Due to these advantages, many researchers have investigated air-based cooling methods for EV batteries, particularly lithium-ion batteries. R. Mahamud et al. [64] numerically studied the effect of reciprocating airflow on the temperature distribution of LIBs. This system utilized flip door valves and a unique duct design, as shown in Figure 2. They employed a two-dimensional computational fluid dynamics (CFD) model, a lumped-capacitance thermal model for the battery cells, and a flow network model. Additionally, their results revealed that the cell temperature difference decreased by  $4\text{ }^{\circ}\text{C}$ , and the maximum temperature surface decreased by  $1.5\text{ }^{\circ}\text{C}$  during a reciprocating period of 120 s.

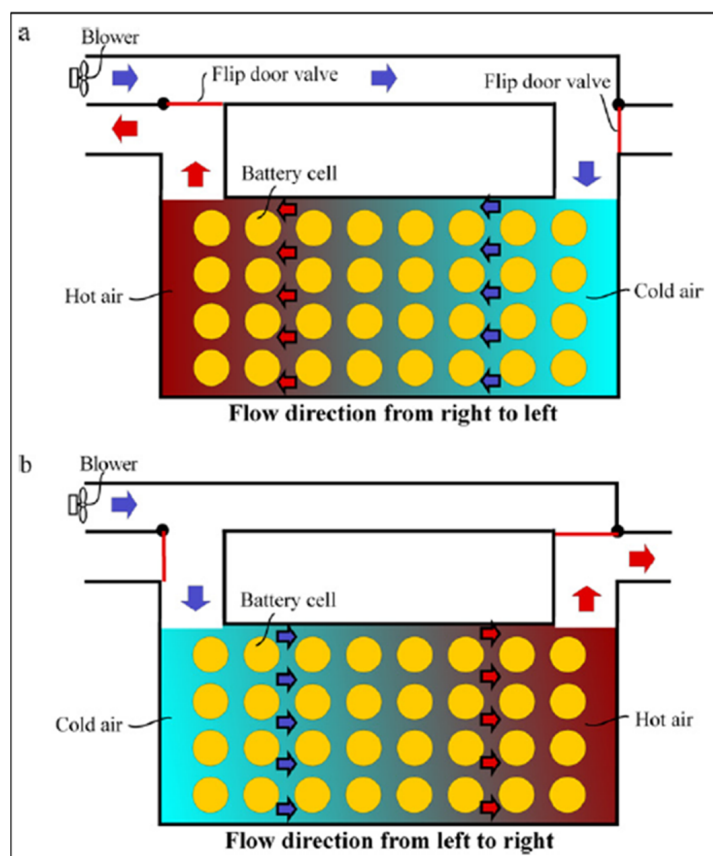


**Figure 2.** Schematic diagram of reciprocating flow (a) from left to right and (b) from right to left [64]. The blue and red arrows represent the cold and hot air flow directions respectively, while the circles represent the batteries.

Wang et al. [65] conducted a numerical study on the impact of forced air, examining various cell arrangements and fan locations on battery temperature distribution in three dimensions. Their findings indicated that placing the fan at the top of the battery yielded the best results, regardless of the arrangement used for the pack. Moreover, while the

cubic arrangement offered the best balance of cost and cooling behavior, the hexagonal arrangement provided optimal utilization of pack space along with cooling efficiency. Additionally, Chen et al. [66] studied the optimization of U-type airflow structures; it can be noticed that increasing the width of the inlet and outlet reduced the temperature difference ( $\Delta T$ ) and maximum temperature ( $T_m$ ). Wang et al. [67] experimentally studied the effects of forced air cooling with varying charge and discharge rates on LIBs. Their results indicated that higher charge and discharge values were ineffective under forced air cooling due to increased  $\Delta T$  and  $T_m$ . Gocmen et al. [68] numerically investigated the effect of using elevated battery positions on the  $\Delta T$  and  $T_m$  of a battery pack of higher discharging rates subjected to forced airflow, as shown in Figure 3. They found that uniform temperature could not be maintained at discharge rates greater than 6C without incorporating fins, effectively reducing  $\Delta T$  and  $T_m$ .

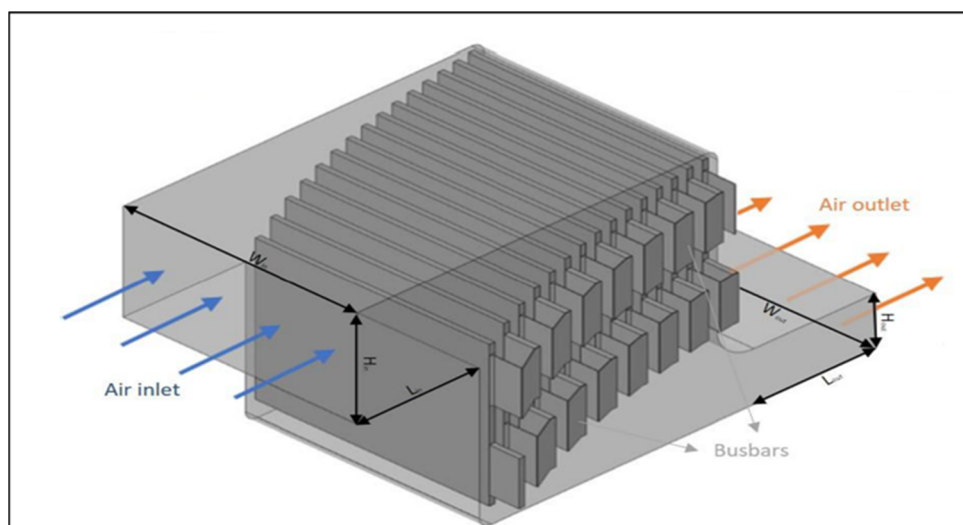


**Figure 3.** Schematic diagram of battery pack [68].

Lazim et al. [69] explored the impact of three different flexible baffle configurations within a battery pack under various airflow rates. Their analysis showed that the staggered configuration significantly reduced the  $\Delta T$  and  $T_m$  at an inlet velocity of 1 m/s with a 4 mm space between the batteries. Based on the preceding literature review, it is evident that air cooling is not a reliable method for maintaining thermal uniformity within the battery pack due to the low specific heat of air. Increasing the number of fans would demand more power and generate higher noise levels, while adding fins would increase the system's overall weight.

### 3.1.2. Liquid Cooling

The homogeneity of the temperature within a battery pack is one of the most crucial factors influencing the lifespan and efficiency of LIBs [70,71]. One of the primary advantages of liquid cooling is its superior heat transfer capabilities, which allow for a more balanced temperature distribution in lithium batteries compared to air-based cooling solutions [58]. The working fluid plays a pivotal role in liquid cooling systems, and various fluids can be utilized, including oil, water, ethylene glycol, liquid metals, boiling liquids, and nanofluids [59,70]. The choice of working fluid depends mainly on the specific heat transfer rate required to maintain the battery temperature within an optimal range. Liquid cooling systems can be categorized into two types, namely direct and indirect cooling systems. This classification is based on whether the working fluid comes into direct contact with the battery or circulates externally.

- Direct Cooling

The direct cooling of batteries is an effective strategy for transferring heat from the battery cells to the working fluid through physical contact. This heat transfer can occur via sensible heat in a single-phase system or latent heat in a two-phase system. A significant advantage of direct cooling is using dielectric fluids as coolants, which are favored for their performance, safety, and longevity in electric vehicle applications. One notable benefit of this method is its ability to improve the temperature homogeneity of LIBs [71]. Recent studies have focused on various parameters affecting the thermal performance of direct liquid cooling designs.

Tan et al. [72] conducted a numerical analysis to examine the influence of flow direction, channel height, coolant velocity, and the number of channel layers on thermal efficiency and power consumption. Their results indicated that  $\Delta T$  and  $T_m$  were reduced by 18.1% and 25%, respectively, when the channel height was set to 30 mm. In another study, Wu et al. [73] designed a battery pack utilizing silicon oil flow for direct cooling. This design improved the temperature distribution of the LIBs, ensuring that  $T_m$  and  $\Delta T$  remained within the standard operating range at a discharge rate of 1C.

Larrañaga-Ezeiza et al. [74] proposed an innovative approach to direct liquid cooling by immersing lithium-ion pouch cells rather than the entire battery system. As illustrated in Figure 4, this design significantly reduced the mean cell temperature by 6.4 °C, with  $\Delta T$  decreasing dramatically from 5.7 °C to 0.4 °C. Notably, the thermal response during actual driving cycles was rapid, demonstrating effective heat management. Additionally, Giannicchele et al. [75] investigated the effects of low-boiling dielectric liquids on immersed batteries at varying discharge rates. Their experimental findings revealed that direct cooling notably reduced surface temperatures, particularly under higher discharge rates.

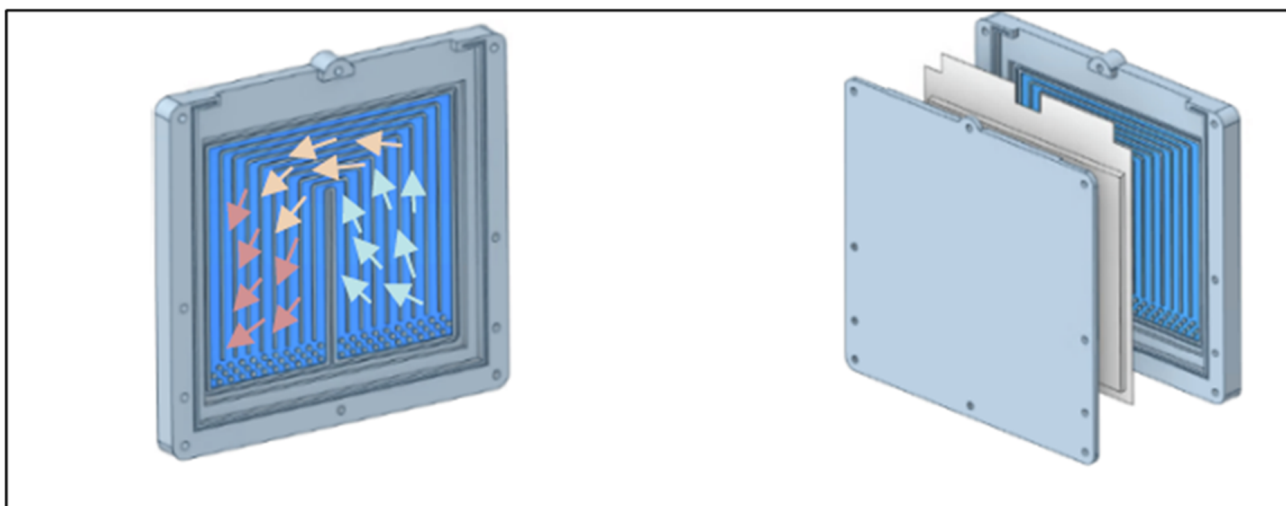


**Figure 4.** Schematic diagram of proposed design of direct liquid cooling [74].

Guo et al. [76] numerically proposed and optimized a multichannel direct liquid cooling system, considering thermal behavior and weight, as shown in Figure 5. The results demonstrated a reduction in  $\Delta T$  to below 36 °C and a  $T_m$  of just 0.65 °C, alongside a decrease in the pack's mass ratio to 10.25%. Moreover, single-phase and two-phase immersion direct cooling methods, such as hydrofluoroether (HFE), significantly enhance temperature distribution in the battery pack, especially at elevated discharge rates [77].

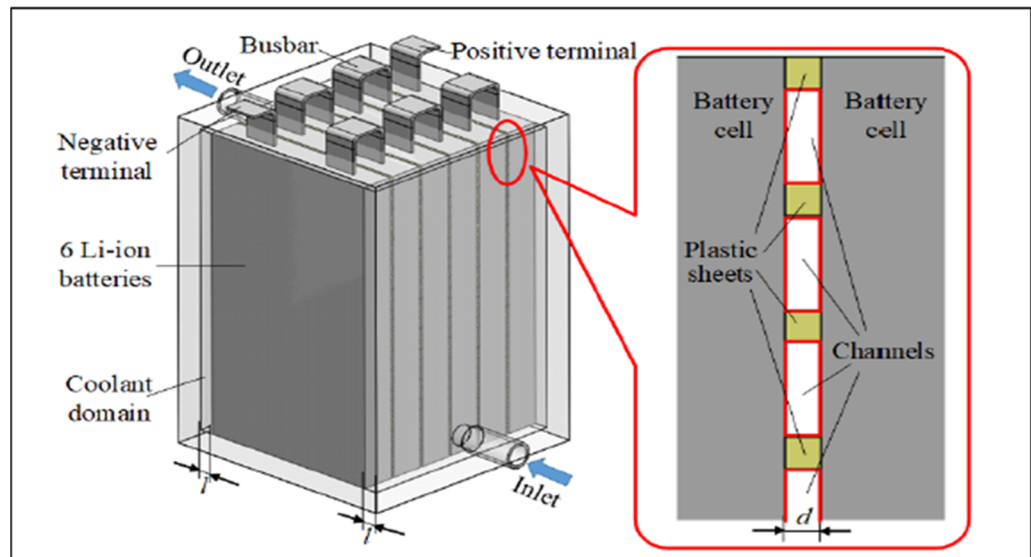


**Figure 5.** Schematic diagram of multi-channel direct liquid cooling [76].

Various operating factors—including the coolant's inlet temperature, discharge rate, and volume flow rate—can significantly influence temperature uniformity. Han et al. [78] examined the impact of mineral oil direct liquid cooling on the thermal and electrical behavior of LIBs, as shown in Figure 6. This study highlighted that lowering the coolest inlet temperature and increasing the volume flow rate resulted in improved thermal behavior. In conclusion, direct cooling is highly suitable for batteries utilized in supercharging and discharging applications. Specifically, at higher charging and discharging rates, cooling immersion effectively maintains the battery within the standard operating temperature range while enhancing temperature uniformity [79].

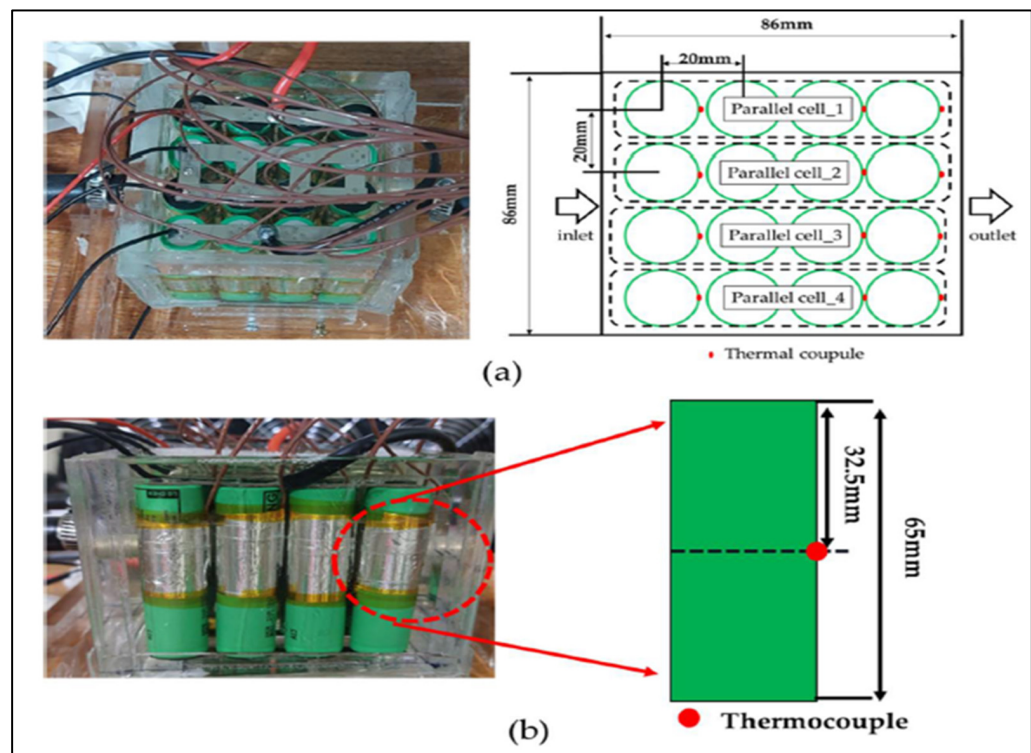


**Figure 6.** The schematic diagram for (a) the battery pack and (b) the location of the thermocouples [78].

- Indirect Liquid Cooling

Indirect liquid cooling is a method that circulates a working fluid to absorb heat from the battery pack without direct physical contact with the cells. Although the design of indirect cooling systems is generally more complex than that of direct cooling, primarily due to incorporating additional components, they offer a reduced risk of leakage, enhancing system reliability [49]. This method ensures higher temperature uniformity across the battery pack, contributing to improved cell performance and longevity. Indirect cooling techniques can be categorized into several types, including cold plates, liquid jackets, mini/microchannels, and nanofluid-based systems. Each approach offers unique benefits and can be tailored to meet the thermal management needs of specific battery configurations.

Liquid cold plates (LCPs) are specialized components that feature inlets and outlets strategically positioned on the surface of battery cells to absorb heat efficiently. Several factors influence the efficiency and effectiveness of LCPs, including the plate's location, design, flow rate, and flow direction. Sheng [50] conducted a numerical study analyzing the effects of double inlets and outlets on the battery pack's temperature uniformity and maximum temperature by comparing five different configurations, as illustrated in Figure 7. The results indicated that at higher flow rates,  $T_m$  and  $\Delta T$  were maintained below 40 °C and 5 °C, respectively, specifically in case 4.1. However, it was also noted that increasing the flow rate correspondingly raised power consumption.

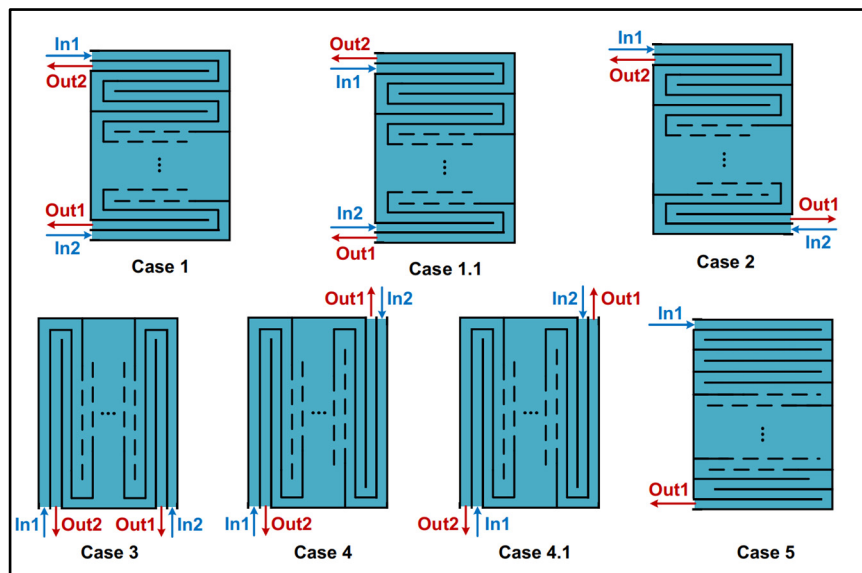


**Figure 7.** The schematic diagram for the seven configurations of the LCP [50].

The design of the LCP significantly affects temperature distribution. Xu et al. [80] conducted a numerical study on the impact of splitter cold plates, considering various parameters such as the number of splitters, angles, distances, lengths, and offsets, as shown in Figure 8. Their findings demonstrated that the splitters' angle and length had the most substantial effect on  $\Delta T$  and  $T_m$ ; increasing these dimensions led to decreases in  $\Delta T$  and  $T_m$ . However, minimizing pump power and friction factors is equally important while modifying LCP designs to enhance heat transfer.

Wang et al. [81] studied and optimized the effects of LCPs on temperature uniformity by incorporating graphite sheet fins and comparing them to aluminum fins. The results indicated that while the liquid flow rate did not significantly impact temperature uniformity, enhancing thermal conductivity with graphite sheet fins notably reduced  $T_m$  and  $\Delta T$ . Moreover, the utilization of graphite fins resulted in a lower weight and volume of the

battery cooling system compared to the aluminum alloy under similar operating conditions. Wang et al. [51] have proposed another innovative LCP design featuring butterfly-shaped channels, as illustrated in Figure 9. This design demonstrated superior performance compared to serpentine, straight, and leaf-shaped channels in terms of temperature uniformity and temperature differentials within the battery pack.

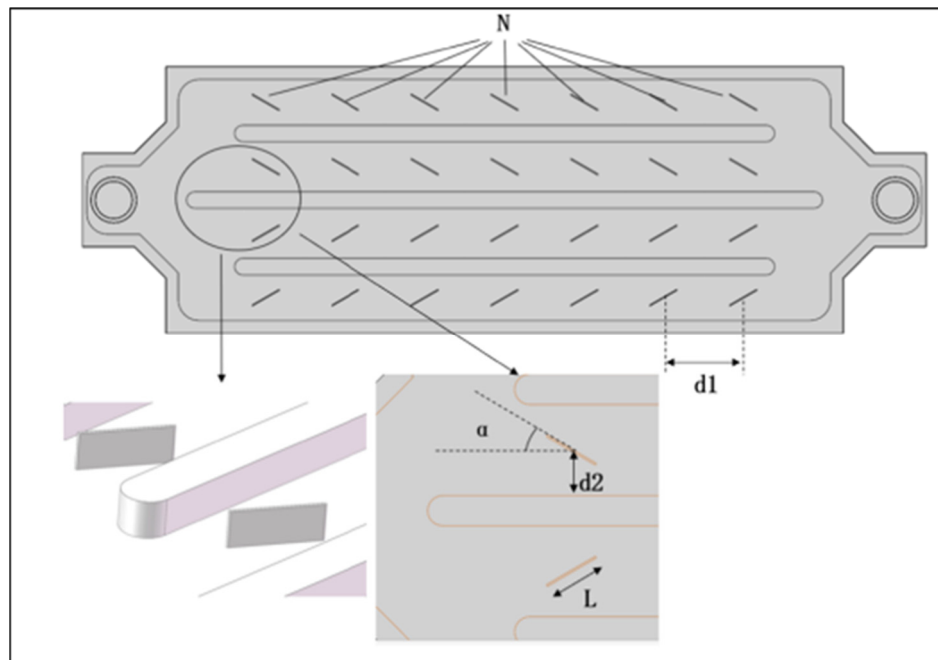


**Figure 8.** The schematic diagram for the LCP with splitters [80].

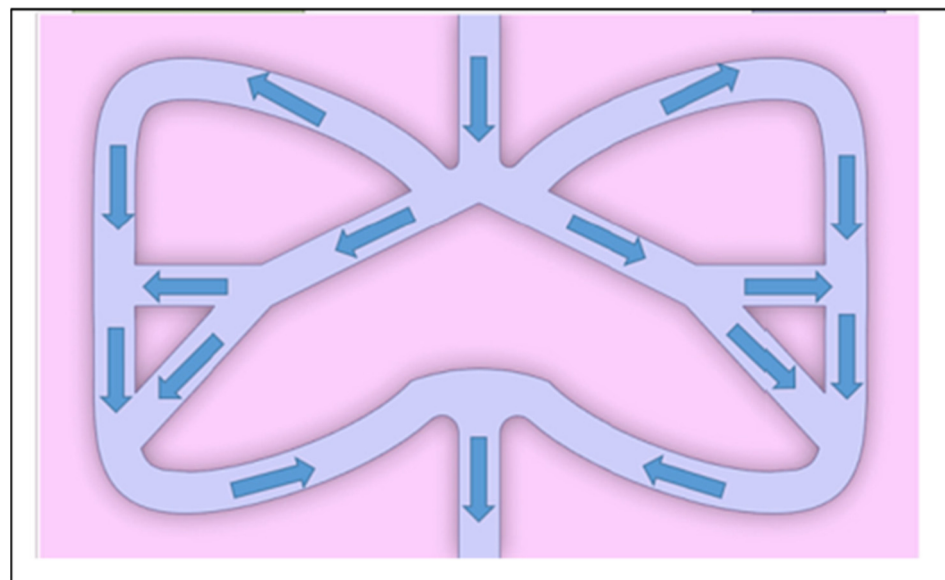


**Figure 9.** The schematic diagram of the butterfly-shaped LCP [51].

Additionally, Rabiei et al. [82] investigated fully embedding LCPs with metal foam microchannels and found that they outperformed both wavy and straight microchannels' cooling performance, although it required the highest pumping power overall. While conventional serpentine LCPs have been widely implemented in battery temperature management, their thermal performance and pumping power can be significant challenges. To address this, Fan et al. [83] explored the effects of an elliptical serpentine LCP integrated

with a grid, as shown in Figure 10. This design achieved the best thermal performance while reducing power consumption by 92.6% compared to traditional serpentine LCP designs. It is well recognized that increasing flow rates reduces the temperature of battery packs; however, there is a practical limit to flow rates, beyond which additional increases yield minimal benefits to thermal behavior [84].

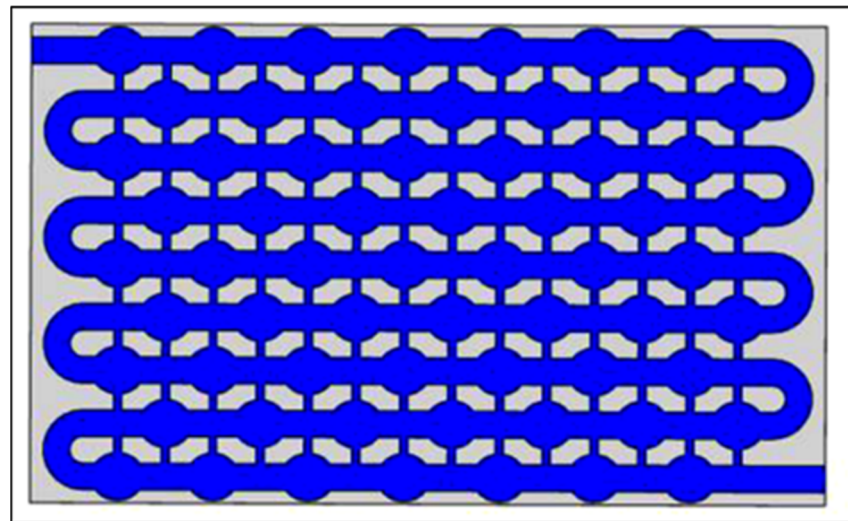


**Figure 10.** The elliptical groove serpentine LCP schematic diagram with a grid [83].

The other type of indirect liquid cooling is the liquid jacket cooling technique. Liquid jacket cooling is employed by utilizing mini channels or cavities, increasing the contact area with the coolant. The efficiency of the liquid jacket strategy is significantly influenced by several factors, including flow rate and direction, the design and number of channels, and the type of working fluid used. Sheng et al. [85] have numerically and experimentally assessed the impact of a cellular liquid cooling jacket on the temperature of LIBs, as illustrated in Figure 11. Their findings revealed that optimizing the flow direction reduced the  $\Delta T$  to less than 5 °C. Moreover, increasing the flow rate brought the  $T_m$  down to below 40 °C while increasing the  $\Delta T$  slightly, but it was still below 5 °C. The authors also noted that while increasing the channel diameter had a limited effect on  $\Delta T$  and  $T_m$ , using a working fluid composed of 50% ethylene glycol and 50% gas effectively reduced  $T_m$  and  $\Delta T$  to less than 5 °C and 40 °C, respectively.

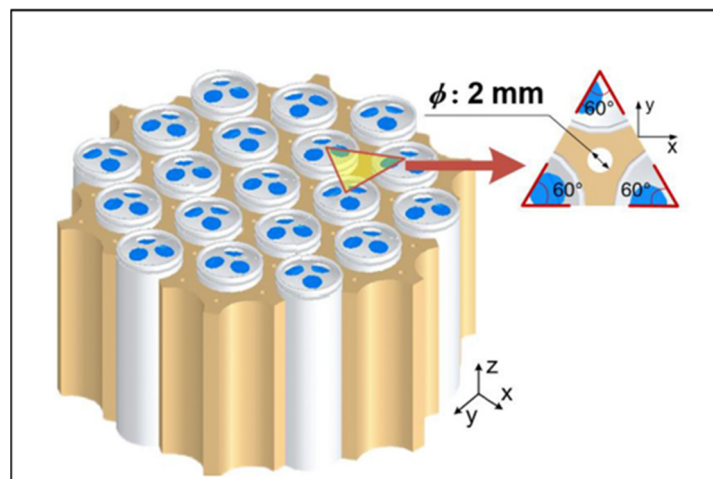


**Figure 11.** The schematic diagram for the cellular liquid jacket [85].

Zhou et al. [86] investigated the effects of a liquid half-helical duct on LIB temperature management, as shown in Figure 12. Their results demonstrated that both the flow rate and helical duct diameter contributed to a decrease in  $\Delta T$  and  $T_m$ , while increasing the number of helical ducts had no significant effect. Particularly, both the flow direction and the pitch of the helical duct were found to have a pronounced impact on reducing  $\Delta T$  and  $T_m$ .

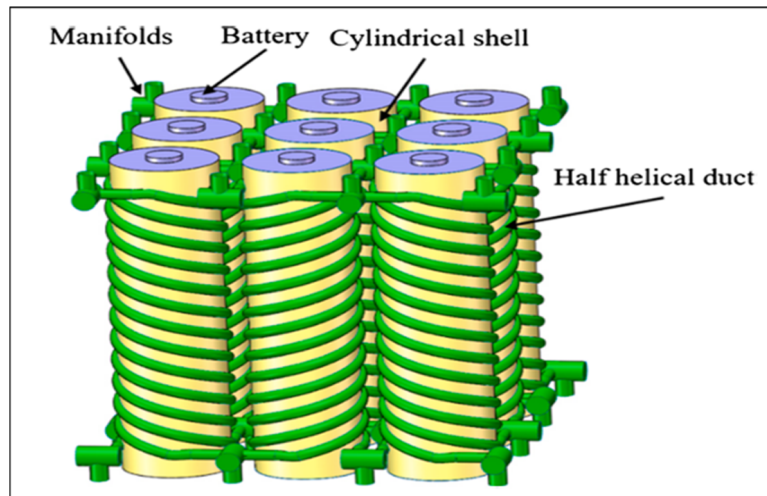


**Figure 12.** Schematic diagram of liquid half-helical duct [86].

The design of the liquid cooling jacket plays an essential role in temperature management. For instance, research conducted by Li et al. [87] indicated that implementing distributed flow via liquid spiral channels resulted in a  $T_m$  of  $34.65\text{ }^{\circ}\text{C}$  and a  $\Delta T$  of  $3.95\text{ }^{\circ}\text{C}$ . Moreover, Sun et al. [88] observed that increasing the channel diameter effectively reduced  $T_m$ , while increasing the height of the liquid jacket slightly elevated  $T_m$ . Overall, expanding the dimensions of the liquid jacket enhanced the cooling performance, underscoring the importance of optimizing design parameters in liquid jacket cooling systems.

Traditional working fluids, such as air, water, and ethylene glycol, have limited effectiveness in enhancing temperature homogeneity and controlling the maximum temperature. As a result, nanofluids have recently emerged as a promising alternative to conventional working fluids. Nanofluids not only improve the thermal conductivity of the working fluid but also increase the heat transfer rate [89]. Nanofluids are created by dispersing solid nanoparticles, typically less than 100 nanometers in size, into traditional base fluids. These nanoparticles can be classified into several categories, including metallic oxide nanoparticles, metallic nanoparticles, hybrid nanoparticles, and carbon-based nanofluids [90,91]. Moreover, mixing the nanoparticles with the base fluids enhances the overall thermal conductivity of the working fluid [92,93], resulting in improved thermal performance. One notable advantage of nanofluids is their ability to reduce the  $T_m$  of the battery pack. However, studies have shown that while nanofluid enhancements can lower  $T_m$ , they do not significantly improve the uniformity of battery temperature [94]. Although increasing the flow rate of the nanofluid can help mitigate the temperature of LIBs to below  $35\text{ }^{\circ}\text{C}$ , this comes at the cost of increased pumping power due to the higher viscosity introduced by the nanoparticles [95]. Furthermore, it has been observed that increasing the concentration of nanoparticles leads to a decrease in the  $T_m$  of the battery pack. This reduction is attributed to enhancing the convective heat transfer coefficient from the nanoparticles' presence [96,97].

### 3.1.3. Thermoelectric Cooling

Thermoelectric coolers (TECs) are solid-state devices that operate based on the Peltier effect. The functionality of a TEC relies on the temperature difference created when an electric current passes through the device, facilitating the transfer of heat from the cold side to the hot side, depending on the direction of the current flow. TECs offer several advantages, including low maintenance requirements, simple structure, and the absence of leakage risks [98]. Studies conducted by X. Cui and S. Jiang [99] and X. Cui and T. Hu [100] investigated the impact of TECs on the uniformity of LIB temperatures, as shown in Figure 13. They implemented four TECs located at different positions within the battery pack. Their findings revealed that installing TECs effectively reduced  $T_m$  and  $\Delta T$  across the battery cells.

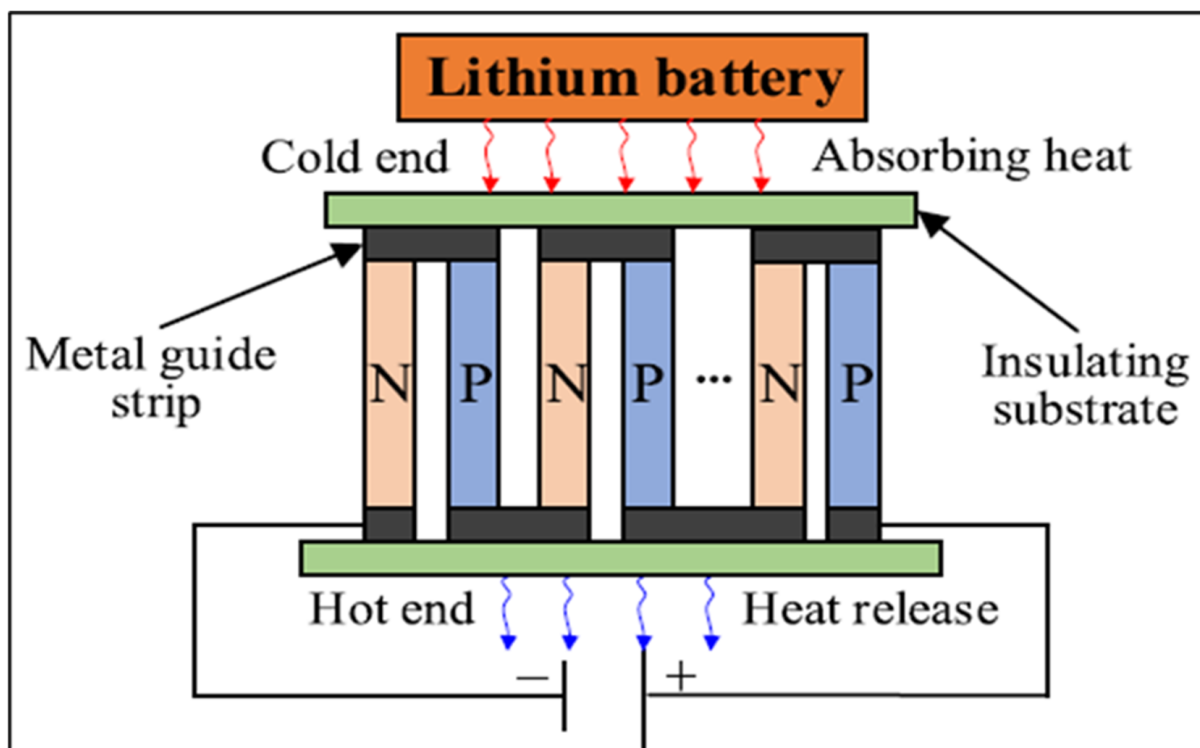


**Figure 13.** Schematic diagram of TEC [100].

Despite these merits, TECs are less efficient, making them less reliable for high charging and discharging rates. Lyu et al. [101] experimentally explored the integration of TECs with liquid cooling systems, as illustrated in Figure 14. Their results demonstrated that this combined approach successfully maintained  $T_m$  below 20 °C at an operating voltage of 40 V for the TEC liquid cooling system. Furthermore, Zhang et al. [61] reported that the TEC liquid cooling configuration not only kept the temperature of the LIBs below 291 K but also improved temperature distribution uniformity.

One critical factor influencing the efficiency of TECs is the cooling of the hot side. H. Sait [102] investigated the effect of nanofluids on the TEC's hot side with various fin cross-sections, as depicted in Figure 15. Their study concluded that increasing the flow rate of the nanofluid, particularly with triangular fins, decreased  $T_m$ , although it was at the cost of an increased pressure drop.

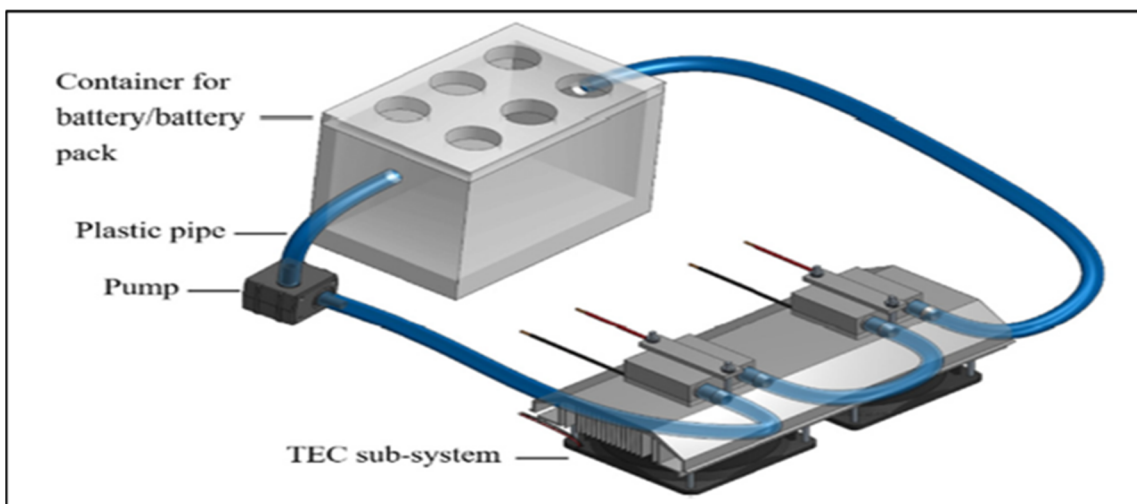


**Figure 14.** Schematic diagram of TEC liquid cooling [101].

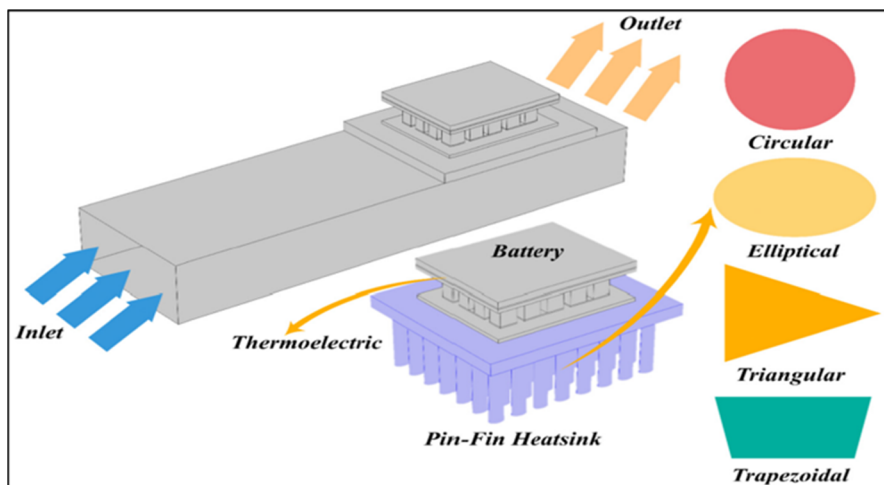


**Figure 15.** Schematic diagram of TEC with nanofluid cooling of heat sink [102].

### 3.2. Passive Cooling

Passive cooling techniques utilize natural processes and the inherent properties of materials to efficiently dissipate heat, optimizing  $T_m$  and  $\Delta T$  within the battery pack without relying on external power sources such as pumps, fans, or compressors. The advantages of passive cooling methods include reduced maintenance costs, minimal noise generation, and extended operational lifespans of the cooling system [103]. Recently, significant research has been directed toward using phase-change materials (PCMs) and heat pipes (HPs) as promising solutions for enhancing passive cooling capabilities, as illustrated in Figure 1. These technologies leverage the thermal dynamics of materials to efficiently absorb and transfer heat, thereby improving the overall thermal management of battery systems.

#### 3.2.1. Phase Change Material (PCM)

PCMs are widely utilized in EVs due to their simple design, energy efficiency, and quiet operation. The principle behind PCMs relies on the absorption and release of latent heat during the transition between solid and liquid states, enabling them to effectively manage heat within a specific melting point range defined by their material properties. PCMs can be classified into pure PCMs and composite PCMs [103]. Pure PCMs include eutectic PCMs, organic PCMs, and inorganic PCMs [104]. Verma et al. [105] found that a layer of fatty acid PCM with a thickness of 3 mm reduced  $T_m$  to 305 K. Huang et al. [106]

studied the effects of the thermophysical properties of PCMs on  $T_m$  and  $\Delta T$  using both experimental and numerical methods, as shown in Figure 16. Their results indicated that while it is beneficial to improve thermal conductivity, too much enhancement could lower the latent heat and density, leading to a higher  $T_m$ .

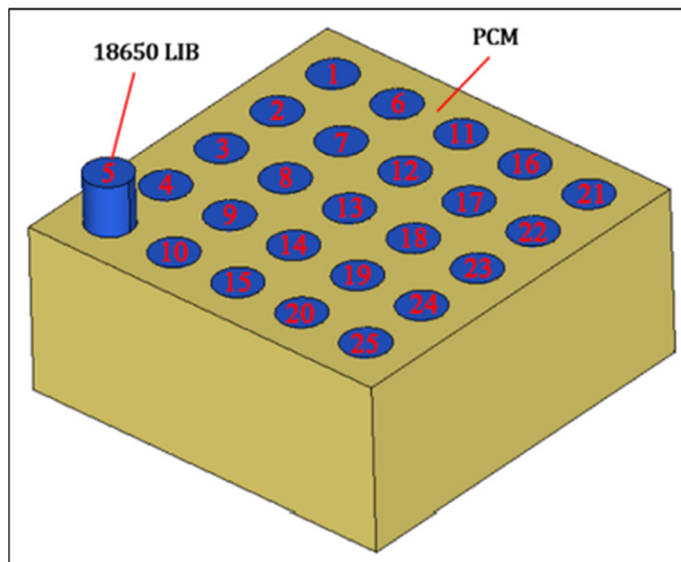


**Figure 16.** The schematic diagram for the LIBs with the metal foam-based PCM [106].

Rajan et al. [107] found that the 1-tetradecanol PCM reduced  $T_m$  by 7 K, as shown in Figure 17. However, the temperature uniformity was not enhanced. Therefore, they also used the metallic PCM (copper foam with 1-tetradecanol), and the result signaled that the temperature homogeneity is better than that of the pure PCM; moreover,  $T_m$  is decreased by 3 K compared with the pure PCM. Even though pure PCMs have a simple structure, they exhibit lower conductivity and stability.

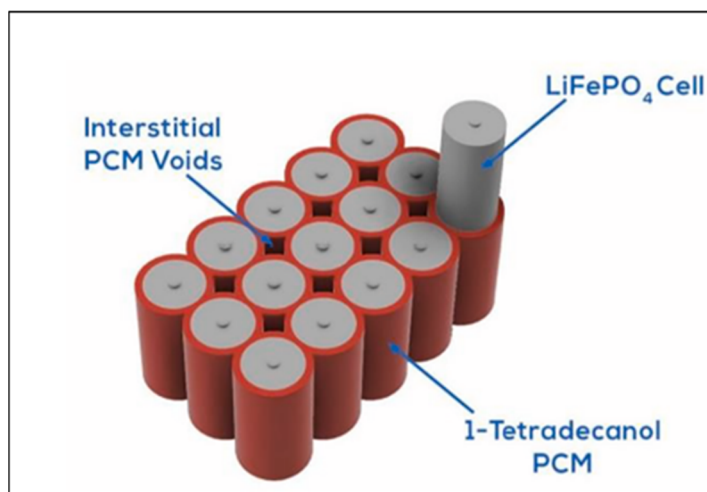


**Figure 17.** The schematic diagram for the LIBs with the 1-tetradecanol PCM [107].

Pure PCMs can act as insulators when reaching full capacity, causing a significant increase in temperature. Conversely, composite PCMs offer higher conductivity than pure PCMs. The conductivity of composite PCMs is enhanced by adding metallic nanoparticles such as copper, aluminum, silver, etc., and carbon-based additives like graphite nanoplatelets, carbon nanotubes, etc., ultimately improving the overall heat transfer properties of the PCM [108]. El Idi et al. [109] found that aluminum foam PCM maintained

a  $T_m$  below 27 °C in LIBs and enhanced the uniformity of the temperature. Moreover, they concluded that the increase in thickness of the PCM does not significantly impact the battery temperature. Jilte et al. [110] applied multi-layers of nanoparticle-based PCM on the LIBs, and they found that even though the ambient temperature was 40 °C, the nanolayer-based PCM maintained a  $T_m$  below 46 °C.

Chen et al. [108] proposed a porous aluminum structure filled with composite PCMs to enhance the thermal behavior of the LIBs, as shown in Figure 18. The study revealed that the  $T_m$  and  $\Delta T$  were below 35 °C and 3 °C, respectively. Behi et al. [111] studied experimentally and numerically the influence of a composite PCM (PCM-graphite) on the maximum and uniformity temperature of the LIBs. They noticed that the  $T_m$  and  $\Delta T$  decreased to 39 °C and 0.3 °C, respectively. Furthermore, Hussain et al. [112] studied metallic composite PCMs (nickel foam/paraffin and copper foam/paraffin). The study showed that metallic composite PCMs enhanced  $\Delta T$  and  $T_m$  compared with natural air cooling and pure PCM. The study showed that, at a discharge rate of 2C,  $T_m$  decreased for copper foam/paraffin and nickel foam/paraffin to 29.5 °C and 30.5 °C, respectively. Moreover, at a discharge rate of 1.5 C,  $\Delta T$  decreased to 0.5 °C and 0.8 °C, respectively.

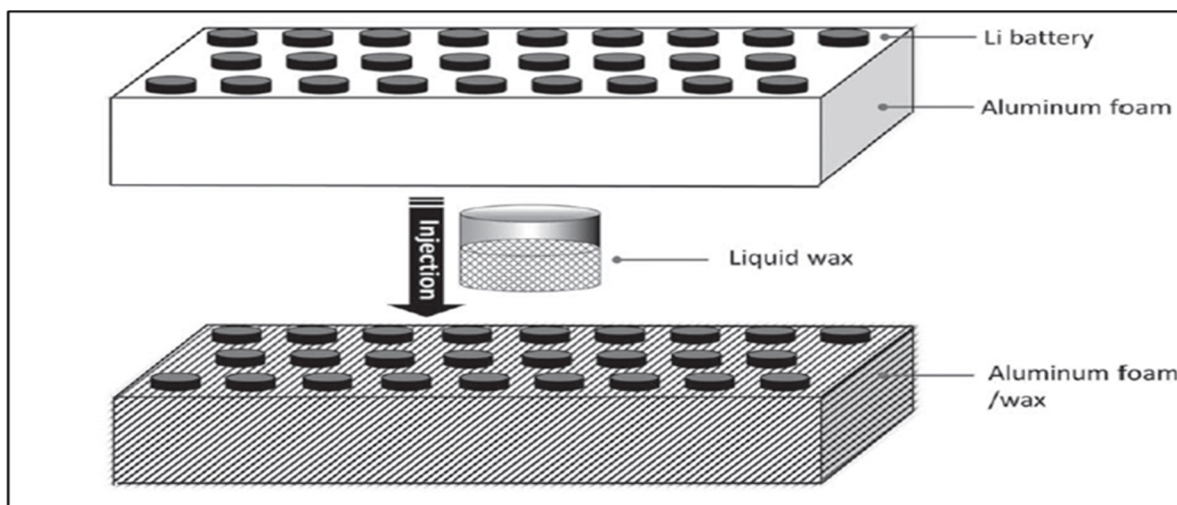


**Figure 18.** The schematic diagram for the LIBs with a porous aluminum structure filled with composite PCM [108].

Budiman et al. [113] demonstrated that up to a discharge rate of two, the paraffin composite PCM maintained the temperature of the LIBs below 45 °C and enhanced the uniformity of the temperature. In conclusion, while PCM-based BTMSs can effectively reduce the temperature and maintain consistent thermal conditions in LIBs, their capability to handle higher discharge rates remains an issue. Additionally, the stability and flammability of PCMs require further investigation. On the other hand, PCMs could be highly effective in hybrid techniques that combine PCMs with active cooling methods, which will be discussed in the sections below.

### 3.2.2. Heat Pipe

The heat pipe device has recently proven to have a better ability to mitigate the temperature of an EV battery. The heat pipe can absorb the heat from the surface of the battery pack by conduction. In addition, its principle depends on the phase change and the capillary action inside the pipe. The working fluid changes from liquid to gas by heat absorption; the phase-change situation depends on the vacuum pressure inside the heat pipe and the saturation temperature and pressure of the working fluid. Depending on the vapor pressure difference and the capillary action, the vapor and the liquid are

driven inside the heat pipe [114]. Moreover, the heat pipe geometry can be classified into three major parts, namely adiabatic, condenser, and evaporator zones [115]. Also, the heat pipe can be categorized based on operating temperature into two types, which are fixed conductance, which is not operating at a constant temperature, and variable conductance, which can maintain a constant operating temperature [116].

The selection of the working fluid is considered vital because it significantly influences the device's performance and efficiency. A HP's most common working fluids are water, acetone, ethanol, nanofluid, etc. [117]. This factor's importance cannot be overstated, as it plays a critical role in determining the heat pipe device's overall effectiveness in managing the EV battery's temperature.

Several researchers have studied the effect of the HP-BTMS on the maximum temperature and the temperature uniformity of the LIBs. Behi et al. [118] studied experimentally and numerically the impact of a heat pipe on the higher temperature zone of lithium titanate (LTO) at a higher discharge rate of 8C. The authors found that the single heat pipe enhanced the cooling load by 29.1%. In addition, to increase the effectiveness of the heat pipe loop, Vachhani et al. [119] studied the effect of the dual evaporator on the  $\Delta T$  and  $T_m$  of the LIBs during different ambient temperatures ( $30^{\circ}\text{C}$ ,  $40^{\circ}\text{C}$ , and  $45^{\circ}\text{C}$ ) and discharge rates (1C, 1.5C, and 2C), as shown in Figure 19. The result revealed that the proposed design decreased the  $T_m$  and  $\Delta T$  below  $60^{\circ}\text{C}$  and  $3.5^{\circ}\text{C}$  at ambient temperature ( $30^{\circ}\text{C}$  and  $40^{\circ}\text{C}$ ) and charging/discharging rates (1C and 1.5C), respectively. It was found that the ambient temperature and inlet of the wind speed only impacted the maximum temperature of the battery pack when using the HP-BTMS with fins.

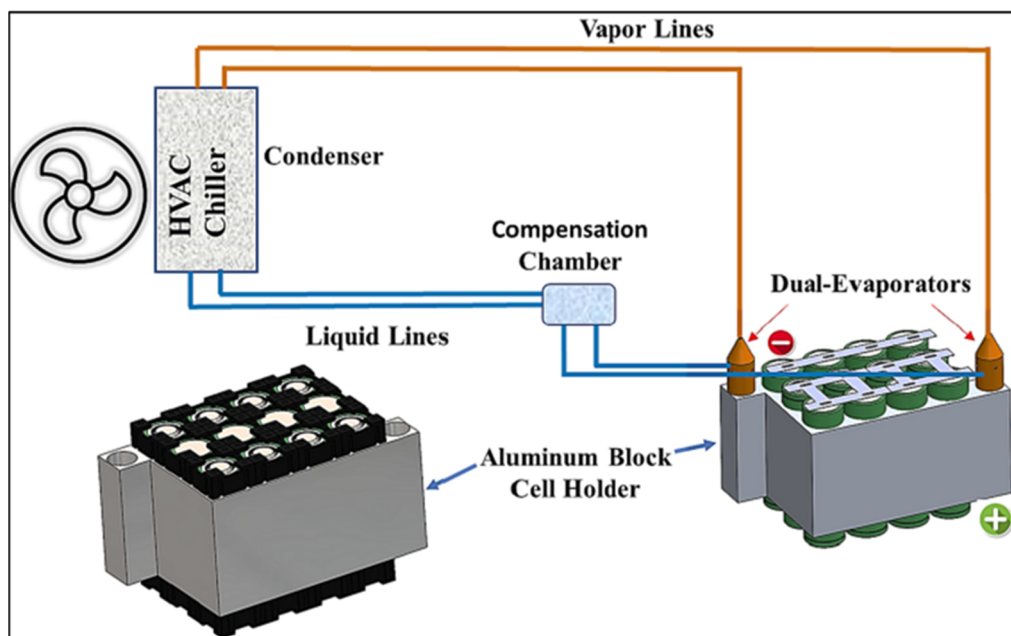


**Figure 19.** The schematic diagram for the dual-evaporator heat pipe loop [119].

On the other hand, the fin spacing influences the uniformity of the battery temperature [120]. The number and design of heat pipes are considered crucial for the thermal performance of the HP-BTMS. Therefore, Nasir et al. [121] showed that increasing the number of heat pipes decreased the battery pack's temperature. However, the number of heat pipes needs to be optimized. Furthermore, the result revealed that the LIB's temperature significantly decreased when the HP's diameter increased.

### 3.3. Hybrid Cooling

Based on the above discussion about the active and passive BTMS strategies, it can be noticed that each approach has its own set of limitations. To address these barriers, researchers have introduced the hybrid BTMS, which integrates the merits of both active and passive techniques. This innovative combination mitigates the drawbacks associated with each method and significantly improves the overall thermal performance of the battery pack and power consumption. Moreover, the hybrid BTMS has a crucial influence on the homogeneity and the consistency of the battery pack temperature. Consequently, the hybrid BTMS has recently been extensively studied.

Liu et al. [122] have investigated the effect of a PCM/copper foam composite with helical liquid channel cooling on  $\Delta T$  and  $T_m$ . Their result pointed out that the melting point of the PCM has the most obvious influence on the temperature of the battery pack. Moreover, the result revealed that below 3C, the increase in inlet velocity decreased significantly, causing a decrease in temperature. However, after 0.05 m/s, it has a minor influence on the thermal behavior. Furthermore, the result showed that liquid cooling influenced the PCM's melting point. Thus, the liquid flow increases the amount of latent heat that the PCM can absorb during the cycle because the helical channels inside the PCM region help absorb the heat from the PCM. Similarly, Fan et al. [123] found that multi-stage Tesla valve liquid cooling with PCMs reduced the  $T_m$  and  $\Delta T$  of the LIBs to 33.12 °C and 1.5 °C, respectively. Moreover, the pressure drop decreased to 647.8 Pa. The integration between liquid cooling and PCMs has shown superior thermal behavior, as shown in Figure 20.

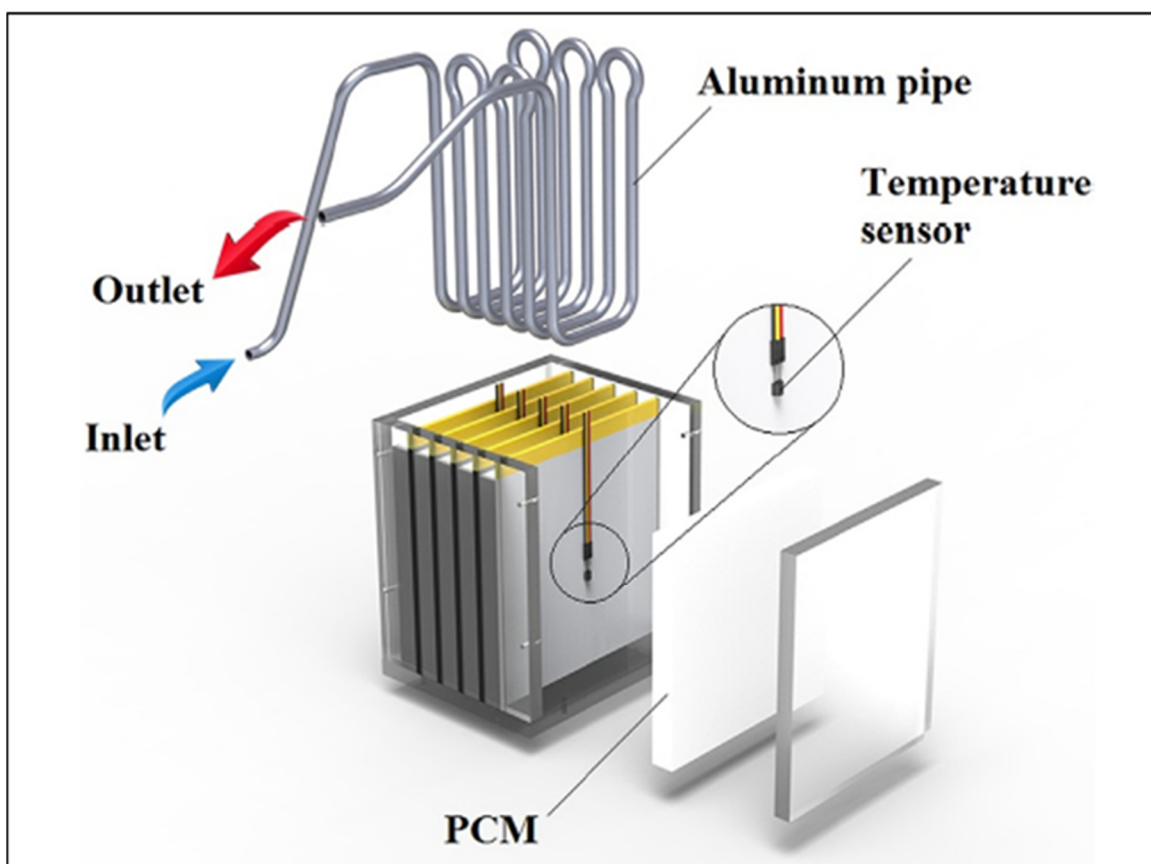
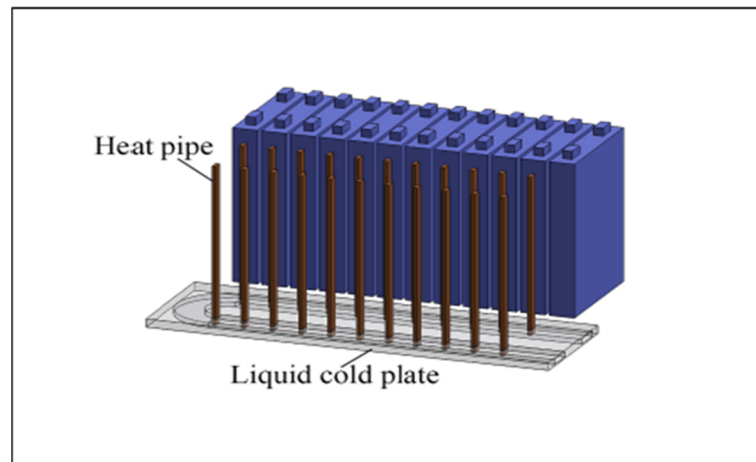


Figure 20. The schematic diagram for the PCM liquid cooling of LIBs [123].

In addition, S. Hekmat [124] investigated the heat pipe with a cold plate, as shown in Figure 21. The HP-LCP decreased the  $\Delta T$  and  $T_m$  by 6.95% and 11.08%, respectively, by optimizing the dimension of the channels compared with the LCP alone. It is well known

that the influence of the geometry of the LCP on the BTM is vital. Zhang et al. [125] found that the L-shaped LCP with a heat pipe maintained a  $T_m$  and  $\Delta T$  below 30.12 °C and 2.02 °C at a 3C discharge rate. Moreover, the study revealed that energy consumption could be reduced from 30% to 97.5% using intermittent liquid cooling instead of continuous liquid cooling with the same thermal performance. Jang et al. [126] found that an increase in the flow rate and a decrease in the temperature of inlet flow reduced  $T_m$ . Additionally, the study showed that with HPs, the consistency of the temperature of the batter pack was enhanced, and  $\Delta T$  was maintained below 5.8 °C for higher discharge rates compared with the LCP only.



**Figure 21.** The schematic diagram of the HP-LCP BTMS [124].

To avoid complexity, air cooling was used with PCMs [127]. It was found that the air–PCM BTMS decreased and enhanced the homogeneity of the LIBs. Moreover, the findings showed that an increase in the airflow rate could reduce the temperature to 25 K. Likewise, it was found that forced air cooling and PCM layers on the body of the cells enhanced homogeneity and decreased the maximum surface temperature of the LIBs, as shown in Figure 22 [128]. However, the result revealed that the cell spacing and the PCM thickness layer need to be optimized to maximize the use of the air–PCM hybrid BTMS.

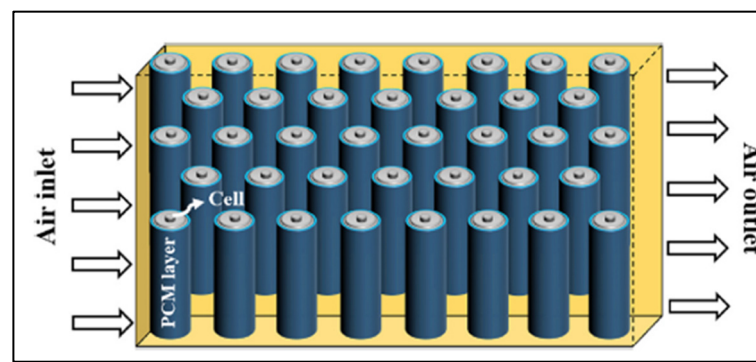


**Figure 22.** The schematic diagram of the air–PCM BTMS [128].

On the other hand, it can be noticed that the air with the HP-BTMS can reduce and enhance the temperature of lithium nickel manganese cobalt oxide (NMC) battery cells [129]. They noticed that the air inlet velocity has a noticeable influence on reducing the maximum surface temperature of the battery pack. It was found that the air path has a vital influence on the temperature uniformity for the HP–air BTMS. Carbajal [130] suggested three paths for the airflow of HP–air BTMS, as shown in Figure 23. The results demonstrated that the

best thermal performance was for the (I) airflow path, which enhanced the temperature's homogeneity and reduced  $T_m$ .

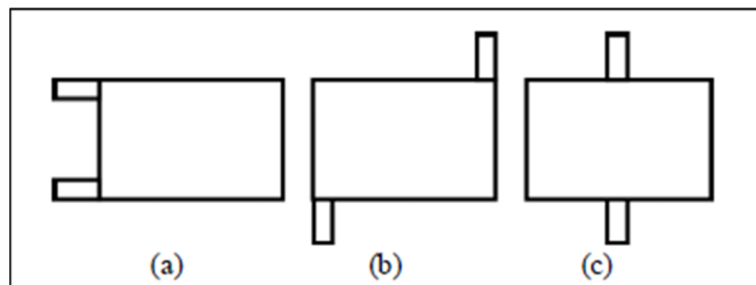


**Figure 23.** The schematic diagram for the proposed air flow path: (a) U path; (b) Z path; (c) I path [130].

One of the best combinations of hybrid strategies is forced convection by air with a liquid BTMS. This combination includes the benefits of active air cooling and active liquid cooling. Saechan et al. [131] proposed forced air with spray liquid cooling using hydrofluoroether (HFE) as a non-electrically conductive cooling fluid, as shown in Figure 24. The authors revealed that the phase change in the liquid droplets with forced air cooling reduced the maximum surface temperature and the temperature difference by  $5.9\text{ }^{\circ}\text{C}$  and  $4\text{ }^{\circ}\text{C}$ , respectively. In addition, Al Tahhan et al. [132] studied the effect of high-speed fans and liquid cooling using an ethylene glycol–water mixture as a working fluid on the battery pack by varying the ambient temperature and discharge rates. It was found that  $T_m$  decreased to  $40.9\text{ }^{\circ}\text{C}$  and temperature uniformity was enhanced.

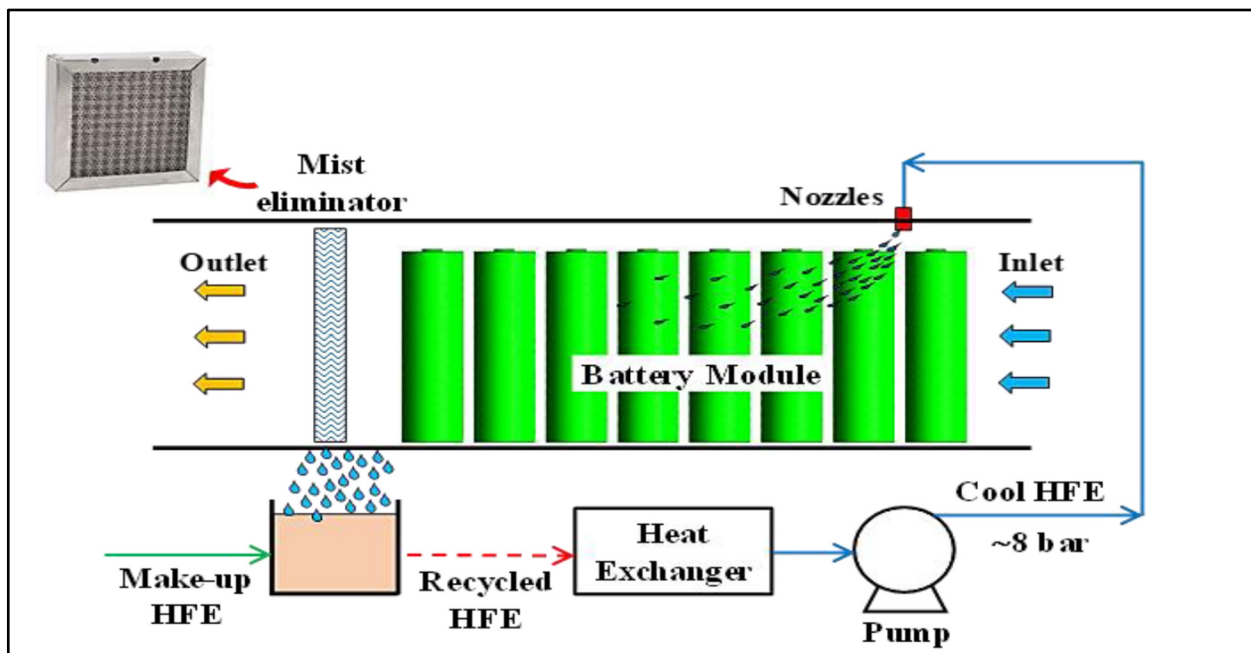


**Figure 24.** The schematic diagram for the air–spray liquid cooling BTMS [131].

Table 1 of this study provides a detailed comparison of various BTMS cooling techniques. The analysis evaluates key parameters such as cooling efficiency, temperature uniformity, energy consumption, weight, cost, complexity, leakage risk, maintenance requirements, thermal conductivity, and compactness.

Table 2 summarizes the advantages and disadvantages of modern temperature control techniques for BTMSs. The hybrid BTMS emerges as a promising solution, combining

the strengths of multiple cooling strategies and enhancing performance and reliability. However, challenges such as design complexity, high cost, and maintenance requirements must still be addressed. In contrast, despite their established use, conventional air and liquid-based cooling systems face inherent limitations, including poor thermal homogeneity (in air cooling) and leakage risks (in liquid cooling), restricting their long-term viability. Meanwhile, passive methods like PCMs and heat pipes offer energy-free operation and stable temperature distribution but struggle with slow heat dissipation and cost inefficiencies. Though compact and maintenance-free, thermoelectric cooling remains constrained by high power consumption and low efficiency. While hybrid systems represent a forward-looking approach, further research is needed to optimize their feasibility, just as emerging air- and liquid-based innovations require deeper investigation to assess their true potential for thermal efficiency.

**Table 1.** Comparative BTMS cooling technique evaluation.

Parameters	Air Cooling (Forced/Natural)	Direct Liquid Cooling	Indirect Liquid Cooling	PCM (Pure/Composite/Metal Foam)	Heat Pipe (Single/Dual Evaporator)	Thermoelectric (TEC + Liquid/Air)
Cooling Efficiency	Low	Moderate	High	Low	High	Low
Temperature Uniformity	Poor	Moderate	High	High	High	Good
Energy Consumption	High	Low	Low	None	Low	High
Weight	Light	High	High	High	High	Light
Cost	Cheap	Medium	Medium	High	High	High
Complexity	Simple	Complex	Complex	Complex	Complex	Moderate
Leakage Risk	None	High risk	High risk	Low	Low	None
Maintenance	Low	High	Medium	High	Low	Low
Thermal Conductivity	Low	High	High	Low	High	Moderate
Compactness	High	Low	Low	Low	Low	Moderate
Key Limitations	Low heat capacity	Leakage, corrosion	Leakage, corrosion	Low conductivity, bulkiness	High cost, design constraints	Low COP, high power

**Table 2.** Advantages and disadvantages of active, passive, and hybrid BTMSs.

Cooling Method		Advantages	Disadvantages
Active	Air-based	<ul style="list-style-type: none"> <li>• Ease to maintain</li> <li>• No leakage risk</li> <li>• Simple design</li> <li>• Low cost</li> <li>• Lightweight</li> <li>• Compact</li> </ul>	<ul style="list-style-type: none"> <li>• High noise</li> <li>• High power consumption</li> <li>• Poor homogeneity of temperature</li> <li>• Low thermal conductivity and heat capacity</li> </ul>
	Liquid-based	<ul style="list-style-type: none"> <li>• High heat capacity</li> <li>• High thermal efficiency</li> <li>• Excellent temperature uniformity</li> <li>• High thermal conductivity</li> </ul>	<ul style="list-style-type: none"> <li>• Complex design</li> <li>• Higher cost</li> <li>• Leakage/corrosion risk</li> <li>• Expensive</li> <li>• Bulk system</li> <li>• High maintenance</li> </ul>
	Based on thermoelectric method	<ul style="list-style-type: none"> <li>• Lightweight</li> <li>• Low maintenance cost</li> <li>• No leakage risk</li> <li>• Compact/no moving parts</li> </ul>	<ul style="list-style-type: none"> <li>• Higher power consumption</li> <li>• Low thermal efficiency</li> <li>• Expensive</li> </ul>

**Table 2.** Cont.

Cooling Method		Advantages	Disadvantages
	Free convection	<ul style="list-style-type: none"> <li>• Simple design</li> <li>• Free power consumption</li> <li>• Easy maintenance</li> <li>• Low cost</li> </ul>	<ul style="list-style-type: none"> <li>• Low thermal conductivity</li> <li>• Low thermal efficiency</li> <li>• Non-uniform temperature distribution</li> </ul>
Passive	PCM-based	<ul style="list-style-type: none"> <li>• Lightweight</li> <li>• Long lifespan</li> <li>• Good temperature distribution</li> <li>• Simple structure</li> <li>• High efficiency</li> </ul>	<ul style="list-style-type: none"> <li>• Not easy to maintain</li> <li>• Low heat transfer coefficient</li> <li>• Not effective for rapid temperature change</li> <li>• Expensive</li> </ul>
	HP-based	<ul style="list-style-type: none"> <li>• No power consumption</li> <li>• Low maintenance</li> <li>• Lightweight</li> <li>• High thermal conductivity</li> <li>• Good temperature distribution</li> </ul>	<ul style="list-style-type: none"> <li>• Leakage risk</li> <li>• Constant design</li> <li>• Low heat capacity</li> <li>• Low thermal efficiency</li> <li>• Expensive</li> </ul>
Hybrid		<ul style="list-style-type: none"> <li>• Combination of advantages of other BTMS types</li> <li>• High-temperature homogeneity</li> </ul>	<ul style="list-style-type: none"> <li>• Complex design</li> <li>• High cost</li> <li>• Maintenance challenges</li> </ul>

#### 4. BTMSs Using AI and ML

The growing reliance on AI across industries has extended to battery thermal management systems (BTMSs), which integrate power electronics, control algorithms, and circuit components to optimize temperature regulation, cell balancing, voltage protection, state-of-charge (SoC) management, and battery lifespan [133].

AI has several subfields, each with a different contribution and diverse applications, such as machine learning (ML), as shown in Figure 25. ML is considered the backbone of AI progression, where algorithms allow the system to learn from the data input to the system, which can then be used to predict the desired output of the system [134]. ML can be categorized into supervised, unsupervised, and reinforcement learning [135].

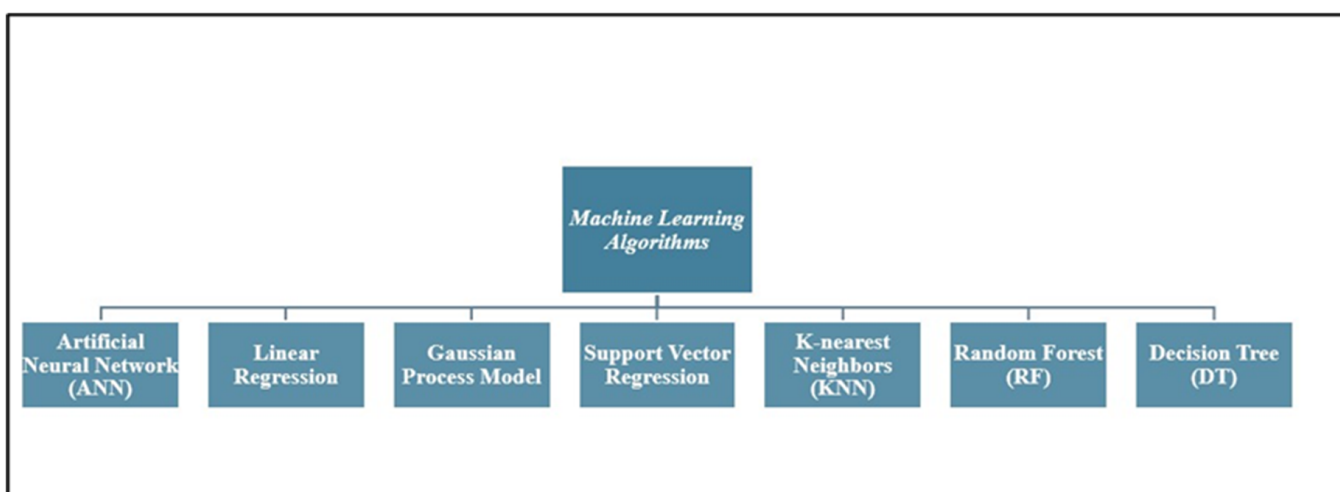


**Figure 25.** Types of machine learning algorithms.

In supervised learning, an output-predictive algorithm is trained on a labeled dataset. Every training dataset in supervised learning consists of an input object and the intended accurate output value. The new dataset is mapped using the extrapolation function that the supervised learning system creates after analyzing the original dataset [135]. Supervised learning is typically applied to regression and classification tasks. For temperature prediction and thermal management, supervised learning methods such as Bayes classifiers, artificial neural networks, decision tree regression, least squares regression, random forest regression, k-nearest neighbors regression, and linear regression are frequently employed [135].

Unsupervised learning uses an unlabeled dataset to extrapolate a function that characterizes the unidentified dataset's structure [135]. The algorithm identifies patterns or sets boundaries to distinguish subsets within a dataset. Unsupervised learning is typically utilized for clustering applications and generative modeling [136]. In an unpredictable environment, reinforcement learning learns by making errors and trying again until it reaches its goal. It is especially helpful when decisions must be made consecutively and actions have gradual, non-obvious results [137]. Recent research highlights AI/ML's potential to enhance BTMS efficiency and adaptability. This section reviews the key studies and methodologies of these algorithms in BTMSs.

The integration of AI and ML into BTMSs is pivotal for optimizing thermal performance and ensuring battery longevity [138]. AI/ML algorithms enable real-time monitoring and predictive control of battery temperatures, mitigating risks such as thermal runaway and uneven heat distribution that degrade performance [138]. By gathering and analyzing the operational data such as temperature, C-rate, and SoC, these techniques are dynamically able to adjust cooling strategies by regulating the flow rates and temperatures of the cooling fluids to maintain cells within their optimal operating range (15–35 °C) and minimize temperature gradients (<5 °C) [24,25]. This proactive thermal regulation not only preserves the critical parameters such as energy density, internal resistance, and cell efficiencies but also extends battery lifespan by reducing the possibility for capacity fade and maintaining the SoH within the acceptable range during the operating period [138].

#### 4.1. Active BTMSs

Active cooling strategies such as forced air convection and liquid cooling have many merits that offer superior heat dissipation capabilities compared to passive systems [139,140]. Although they enhance the uniformity and homogeneity of a battery pack's temperature, especially in LIBs, many key factors influence active cooling strategies, including the velocity flow rate and the ambient temperature of the coolant, as well as the geometry of the cooling system and the space between the cells. These factors significantly impact the battery's thermal behavior, and they need to be optimized to enhance the efficiency and performance of the battery pack. Therefore, to optimize cooling system design and operating parameters, researchers have increasingly adopted AI and ML algorithms for real-time thermal monitoring and predictive analysis in BTMSs [140].

Cell spacing is a key factor that impacts the thermal performance of air-based BTMSs. Therefore, Ghafoor et al. [141] studied and optimized the cell spacing of an air-BTMS using a genetic algorithm and machine learning. They used a genetic algorithm integrated with a support vector machine as a part of the machine learning due to its capabilities in solving nonlinear dynamic problems. Moreover, the machine learning used data from a CFD simulation, which was compared with the experimental data. The result revealed that the optimized design of the cell spacing decreased the  $T_m$  by 3.5 K, and the homogeneity of the cells' temperature was enhanced by 70%. Similarly, Qian et al. [142] optimized the battery spacing of an air-BTMS using a Bayesian neural network. The CFD simulation result was

used to train the Bayesian algorithm. The result revealed that the optimized battery spacing decreased  $T_m$  and  $\Delta T$  to 5.986 K and 300.511 K, respectively. On the other hand, one of the significant drawbacks of the air–BTMS is the noise generation of the cooling system. Therefore, Xu et al. [143] optimized the thermal and aeroacoustics performance of the battery using CFD and an artificial neural network model. This study considered the inlet velocity of the flow, battery spacing, and varying geometry of the inlet and exit channel (the inclination angle). The 50-layer residual neural network (ResNet-50) was used. Also, the technique for order preference by similarity to the ideal solution (TOPSIS) determined the best optimal values for the operating parameters using the data from ResNet-50. Moreover, ResNet-50 used the data of the CFD model. The findings indicated that the optimal design decreased  $T_m$  and  $\Delta T$  by 10.63 K and 9.41 K, respectively. In addition, the noise level was reduced by 4.6 dB.

On the other hand, Shi et al. [144] studied the effect of adding multiple airflow outputs for the U-type air–BTMS on the uniformity and homogeneity of the battery pack temperature using a 3D CFD model and a fully connected deep network (FCDN). The AI model was trained by using 1095 different designs of the BTMS from the CFD simulation results. In addition, the FCDN examined 765,846 potential structural configurations of the BTMS based on the temperature metrics. The result indicated that  $T_m$  was enhanced by 40.36% and  $T_m$  decreased by 6.22 K compared with the original design using three additional airflow outputs for the U-type air–BTMS. Additionally, the inlet velocity and geometry of the Z-type air–BTMS outlet have been optimized using an artificial neural network [145]. The artificial neural network combines a non-dominated sorting genetic algorithm II (NSGA-II) to determine the optimum  $\Delta T$ ,  $T_m$ , and pressure drop values. The artificial neural network was trained using CFD simulation data. The result revealed that there is a linear relationship between the inlet velocity, temperature, and pressure drop. Moreover, it was found that the inlet velocity significantly influences thermal performance and pressure drop. However, the geometry parameters had less impact on it. Furthermore, the optimal values were 1.96 K, 6.32 K, and 2.82 Pa for the  $T_m$ ,  $\Delta T$ , and pressure drop, respectively.

Even though the air–BTMS showed better thermal performance, the inherent uncertainties about the uniformity of the temperature battery pack are still considered issues. Hence, the liquid–BTMS has recently attracted researchers due to its higher thermal capacity, free noise, and cooling efficiency. However, the liquid-based BTMS faces significant challenges due to higher power consumption requirements. Therefore, Liu et al. [146] employed machine learning to optimize power consumption in LIB immersion cooling systems, considering cell spacing and pack temperature. The study used experimental data to build a verified model using the finite element method (COMSOL). Moreover, reliability-based design optimization using the Gaussian process was used in this study. They pointed out that power consumption was reduced by 90% compared with the base design.

Tang et al. [147] investigated and predicted the performance and effect of the integration between a liquid cooling BTMS with a heat pump air conditioning system (HPACS) in EVs and observed the cooling capacity and the coefficient of performance (COP) using a machine learning algorithm. This study employed support vector regression (SVR) and particle swarm optimization (PSO) using experimental data, and the operating parameters were the compressor speed, ambient temperature, and airflow rate of the external heat exchanger. The study revealed that the COP was enhanced to 2.36 and the inlet temperature of the liquid decreased to 19.8 °C. Moreover, it was found that at an ambient temperature of more than 40 °C, the cooling system could decrease the inlet temperature of the batter's liquid to lower than 25 °C at a compressor speed of 4000 rpm. Furthermore, Zhou et al. [148] studied the thermal performance of the liquid wavy channel–BTMS based on machine

learning, considering the influence of the inlet coolant temperature, cooling channel width, coolant velocity, channel wrapping angle, and charging rate (C-rate). The Gaussian process surrogate model was used, and the data was taken from the simulation using finite elements. The results revealed that the cooling system's energy efficiency was enhanced by 126%, and the  $T_m$  and pressure drop decreased to 27.83 °C and 3.53 kPa, respectively, compared with the base design. Moreover, the decrease in inlet coolant temperature and discharge rate significantly influenced the battery pack's temperature reduction compared with other operating parameters. However, the cooling channel width and coolant velocity had the most significant impact on efficiency.

The working fluid in liquid-based BTMSs critically determines system thermal performance. Addressing this, Kanti et al. [149] developed an experimental random forest model to predict the thermal behavior of both hybrid and mono-nanofluid cooling systems. They used a 50:50 mixture ratio of Al<sub>2</sub>O<sub>3</sub> and CuO nanoparticles with water-based fluid. The operating parameters were the coolant flow rate and the discharge rate. It was found that at a 0.5 nanoparticle concentration of the hybrid nanofluid and flow rate of 350 mL/min, the temperature of the LIBs decreased by 54.23%. Moreover, the result revealed that the predicted model of the random forest had exceptional predictive accuracy. Identifying hotspot regions in battery packs is critical, as they reveal poor thermal homogeneity in cooling systems. Therefore, Afzal et al. [150] employed X-gradient boosting (XGB) and decision tree algorithms to predict hotspot locations and intensity. Their results demonstrated significant reductions in hotspot severity with increased coolant velocity and optimized spacing configurations, while the aspect ratio showed a negligible impact on hotspot mitigation.

A comprehensive review of active BTMS studies employing AI/ML techniques is presented in Table 3, which outlines each study including the authors, year, BTMS type, AI/ML algorithm used, input parameters, research objectives, major findings, and gaps.

#### 4.2. Passive BTMSs

The passive BTMS, including heat pipes and PCMs, has shown good thermal performance with lower power consumption. However, optimizing these systems to maintain temperature uniformity remains a challenge. ML and AI have emerged as powerful tools for predicting and enhancing passive BTMS performance.

Jalilantabar et al. [151] proposed a predicted model for the thermal performance of LIBs using a PCM-BTMS based on artificial neural networks to tackle this issue. In this study, the discharge rate, time, PCM type, and PCM thickness were considered the input parameters, and the output parameter was the battery's temperature. The findings revealed that the predicted model showed a good match result compared with the experimental temperature result, with an  $R^2$  value close to one. On the other hand, Khaboshan et al. [152] studied and optimized a BTMS using a PCM, metal foam, and fins using computational fluid dynamics and an artificial neural network. The input parameters were the number of fins, height, length, and time, while the output parameters were the liquid fraction of the PCM and battery surface temperature. The multilayer perceptron was trained with data obtained from CFD simulations. The result demonstrated that the battery surface temperature was reduced by 3 K. Moreover, the model had good predictive capabilities with  $R^2$  values of 0.98.

Arif et al. [153] proposed a model to predict and assess the performance of the PCM-BTMS using a multilayer perceptron (MLP). The input parameters of the MLP model were the temperature of the inner heat sink of the heat sink. Moreover, the output parameter was the liquid fraction. The MLP was trained using data from a segment of the radial heat sink. The proposed model achieved superior accuracy, with a correlation of up to 0.99 compared with LSTM, CNN, and CNN-LSTM. In addition, Anooj et al. [154] studied the influence of

the heat flux variation on the liquid fraction of PCM-BTMS using recurrent neural networks (RNNs). The training data of the RNN model from the simulation considered various types of heat flux, including constant, pulsating, random, wiener, and discharging. Moreover, the numerical model was verified with the experimental result. The temperature was the input parameter, and the liquid fraction was the target of the RNN model. The proposed model had higher prediction accuracy, varying the heat fluxes up to 0.99 and taking less computational time than the numerical result obtained for the liquid fraction.

A comprehensive review of passive BTMS studies employing AI/ML techniques is presented in Table 4, which outlines each study including the authors, year, BTMS type, AI/ML algorithm used, input parameters, research objectives, significant findings, and gaps.

#### 4.3. Hybrid BTMSs

The hybrid BTMS merges multiple cooling approaches for balanced performance, with AI/ML increasingly employed to optimize operating parameters. Sui et al. [155] used a multi-objective optimization approach to improve BTMS performance. The BTMS design included hybrid manifold channels for liquid cooling, with fluid flow and heat transfer methods evaluated using CFD simulations, as shown in Figure 26. The NSGA-II algorithm was also used to investigate the trade-offs between cooling efficiency and pressure drop. This model was critical to determine the best configurations for the manifold channel designs and flow rates. The study found that a maximum battery temperature of 30.73–33.78 °C can be achieved with a cooling pressure drop of 7.66 kPa to 1.76 kPa and a heating power of 10 kW/m<sup>3</sup> for the cell. Additionally, TOPSIS identifies the ideal design configuration, limiting the maximum battery temperature to 45 °C at a discharging rate of 3C and maintaining a pressure drop below 4.2 kPa.

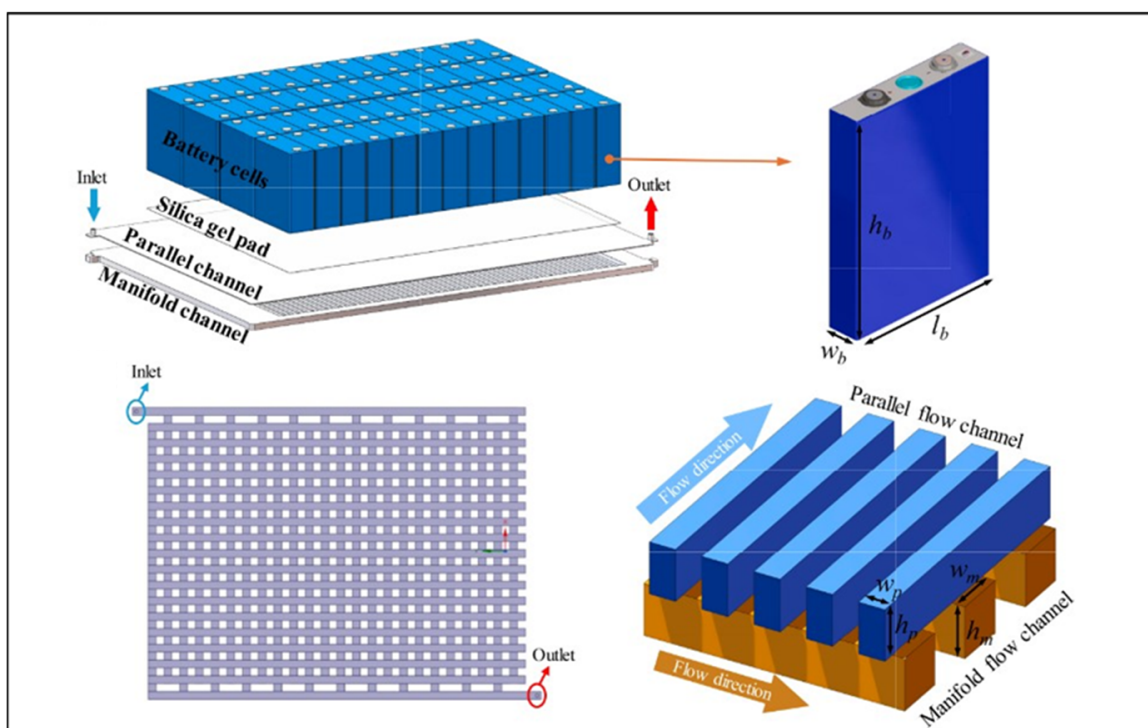


**Figure 26.** A schematic for the CFD design [155].

Khaboshan et al. [152] integrated a hybrid BTMS using phase-change material, metal foam, and fins with the artificial neural network (ANN) model. The study investigated various hybrid BTMS configurations to reduce battery temperature during 3C.

**Discharge in varying situations:** Using a parametric approach, the study investigated how different BTMS material combinations and fin lengths affect system performance. For the CFD simulation, the authors made four cases for this purpose. The first case used only pure PCM, the second case PCM with fins, the third case PCM with metal foam, and the fourth case PCM with metal foam and fins. The ANN model was developed using numerical data from the optimum-designed BTMS situation (fourth case). The data was gathered from the BTMS under challenging environmental conditions (305 K) to include the PCM in solid and liquid forms at a discharge rate of 3C. The numerical simulations generated 52,326 datasets, separated into two sets for training (80%) and testing (20%). The results revealed that combining all three passive cooling approaches resulted in the lowest battery temperature, with a 3 K drop compared to systems using simply PCM. Furthermore, employing the ideal BTMS setup with copper metal foam and fins reduced temperature variance in the battery by about 75% and 66% under normal and challenging climatic conditions, respectively. Furthermore, the model successfully predicted PCM liquid fraction and battery temperature with high R-squared values of 0.98 and 0.99, respectively.

Another research study by Ye et al. [156] investigated a hybrid machine learning method for optimizing a hybrid BTMS with PCM and liquid cooling, as shown in Figure 27. The researchers applied a backpropagation neural network (BPNN) algorithm and sorting genetic algorithm-II (NSGA-II) to predict essential performance characteristics such as maximum battery temperature, standard temperature differential, and system pressure drop. The model was trained using data mining approaches, resulting in a correlation coefficient ( $R$ ) of 0.99988 and a mean square error (MSE) of  $9.5185 \times 10^{-6}$ , demonstrating high accuracy. Moreover, this prediction model was optimized using the non-dominated NSGA-II to improve cooling efficiency, temperature uniformity, and pressure drop. The data for the machine learning model were obtained from numerical simulations of battery cooling systems, emphasizing variables such as battery spacing, cooling tube diameter, and intake velocity. The optimization resulted in a 0.22 K decrease in maximum temperature, a 0.18 K reduction in temperature differential, and a 95.7 Pa reduction in pressure drop. Consequently, the system's energy efficiency was improved by removing 55.17% of the pressure drop.

Guo et al. [157] presented a hybrid BTMS that uses indirect liquid cooling and forced air cooling to improve temperature control in LIBs. The process involves applying deep learning, primarily a long short-term memory (LSTM) model, to anticipate the system's temperature distribution and thermal behavior. This machine learning model was trained using data from hybrid cooling system experiments, including the coolant flow rate, air velocity, and battery charge–discharge cycles. Using a deep learning model based on LSMT with gelu, tanh, and sigmoid activation functions resulted in 99.1%, 98.3%, and 98.7% prediction accuracies, respectively. All of these activation functions have a high capacity for prediction. The sigmoid function outperforms others regarding test accuracy and prediction curve fluctuation. Furthermore, increasing the diameter of liquid cooling tubes reduces battery temperature and temperature difference, with a recommended diameter of 10 mm. However, the battery's heat dissipation efficiency is inadequate due to its distance from the liquid cooling channels. Moreover, the optimum cooling effect is obtained when the forced air-cooling direction is from top to bottom under the coolant condition on the same side, and a forced airflow speed of 0.2 m/s has been decided for energy efficiency.

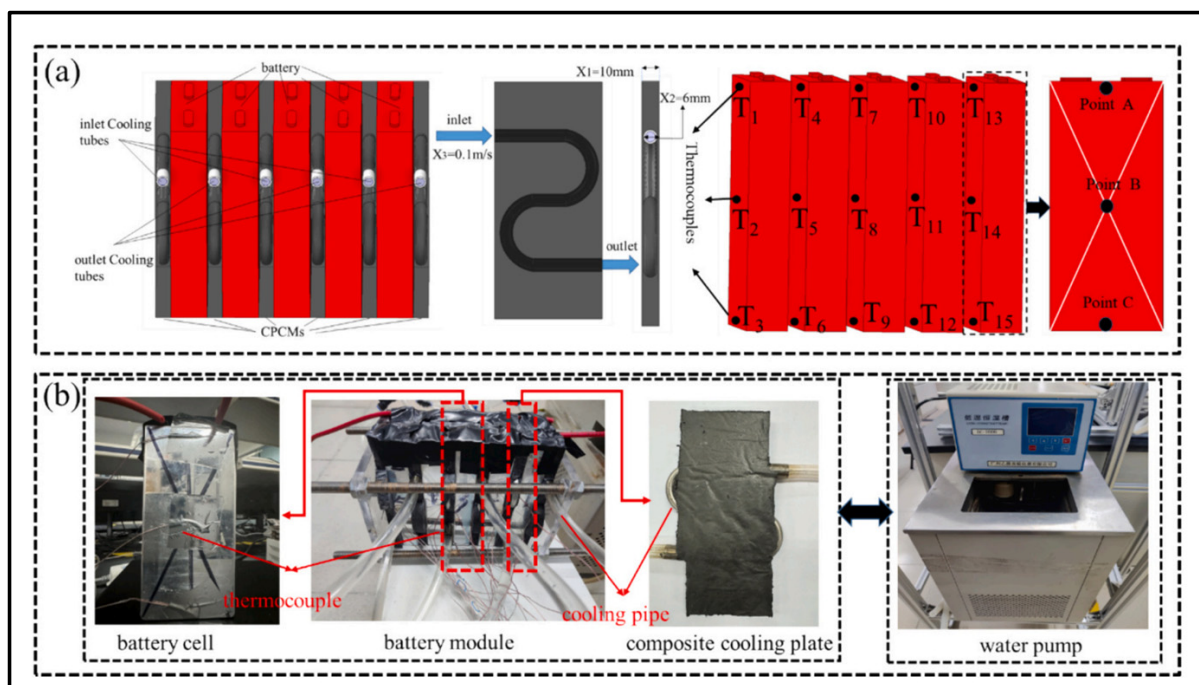


**Figure 27.** A schematic diagram of (a) the battery module structure (b) the experimental setup [156].

On the other hand, Yang et al. [158] designed a hybrid BTMS that combines nickel foam, nano-encapsulated phase change materials (NEPCMs), and aqueous emulsion to improve LIB cooling performance. The authors used CFD simulations to investigate heat behavior and combined them with an ANN machine learning model for predictive analysis. The ANN was trained using CFD-generated data to improve thermal performance by predicting temperature profiles under different scenarios. The key result showed a significant reduction in the maximum battery temperature of over  $40\text{ }^{\circ}\text{C}$  due to the high thermal conductivity of nickel porous media despite a pressure drop of more than 100-fold. Additionally, as the nickel porosity decreased from 1 to 0.97, there was a significant reduction in the maximum temperature of the battery and the pressure drop.

A comprehensive review of hybrid BTMS studies employing AI/ML techniques is presented in Table 5, which outlines each study including the authors, year, BTMS type, AI/ML algorithm used, input parameters, research objectives, major findings, and gaps.

**Table 3.** Summary table of active BTMSs using AI and ML.

No.	Authors	Year	BTMS	AI/ML Used	Input Parameters	Goal/Target	Major Findings	Gaps
1	Monika et al. [159]	2024	Liquid–BTMS	Kriging Model/NSGA II	$L, W_c, \theta, T_{w,in}, \dot{m}_w$	$T_m, \Delta P, h$	$T_m$ increased by 0.07%, $\Delta P$ decreased by 62.32%, and $h$ was enhanced by 64.41%	<ul style="list-style-type: none"> <li>The study considered the ambient temperature and the discharge rate constant.</li> <li>The study focused on the pouch battery type.</li> <li>The results were not experimentally validated.</li> </ul>
2	Zheng et al. [160]	2024	Liquid–BTMS	Artificial Neural Network/NSGA-II	$\alpha, \beta, X1, X2, X3, Y1, Y2, Y3$	$T_m, \Delta T, \Delta P$	$T_m = 34.75^\circ C$ , $\Delta T = 2.26^\circ C$ , $\Delta P = 2562.62 Pa$	<ul style="list-style-type: none"> <li>The study considered one type of battery cell (pouch).</li> <li>The study did not investigate the effect of the ambient temperature variation and the discharge rate.</li> </ul>
3	Yuan et al. [161]	2024	Refrigerant–BTMS	Artificial Neural Networks (Elman–NN)	Compressor speed, ambient temperature, discharge rate, and state of charge	Minimum, maximum, and difference temperature cell	For unexpected condition, predicted model of Elman–NN had maximum prediction error of $0.94^\circ C$ , and maximum MSE and minimum $R^2$ were 0.2275 and 94.48%	<ul style="list-style-type: none"> <li>Other types of geometries of the cooling plate need to be investigated.</li> </ul>
4	Li et al. [162]	2024	Liquid–BTMS	Kriging Model/MOGA	$F, H_c, W_b, W_L, W_S, W_{IO}$	$T_m, VAT, \Delta P$	$T_m = 308.98K$ , $VAT = 306.06K$ , $\Delta P = 520.10 Pa$	<ul style="list-style-type: none"> <li>The study did not consider the effect of the ambient temperature variation and the discharge rate.</li> <li>The results were not experimentally validated.</li> </ul>
5	Al-Haddad et al. [163]	2024	Air–BTMS	Neural Networks	$T_{amb}$ , cell length	Predicted heat flux	Accurate prediction of heat flux and less computational time	<ul style="list-style-type: none"> <li>The study did not consider the effect of the discharge rate.</li> <li>The study did not consider the inlet velocity of the air.</li> <li>The results were not experimentally validated.</li> </ul>

**Table 3.** *Cont.*

No.	Authors	Year	BTMS	AI/ML Used	Input Parameters	Goal/Target	Major Findings	Gaps
6	Bacak [164]	2024	Air-BTMS	Levenberg–Marquardt	$T_{amb}$ , C-rate, $h_{convection}$ , nominal capacity	Surface temperature	ML predicted accurate surface temperature compared with experimental and numerical methods	<ul style="list-style-type: none"> <li>The study focused on one battery cell type.</li> <li>The study was not verified with the experimental work.</li> </ul>
7	Sukkam et al. [165]	2024	Liquid-BTMS	Multilayer Perceptron/GridSearchCV	MaxCh, CR, I, V, SoC, SoH, BT, v, s, H, W, BCL, CL, AC.	Battery health factor	SoC, MaxCh, and BT have a vital influence on battery health factor	<ul style="list-style-type: none"> <li>The study did not consider the effect of ambient temperature.</li> <li>The pressure drop was not studied.</li> </ul>
8	Jiang et al. [166]	2024	Liquid-BTMS	Bayesian Multi-Objective Optimization Algorithm/NSGA-II	$w, d, r$	$T_m, PP$	PP reduced by 71%, $T_m$ reduced slightly	<ul style="list-style-type: none"> <li>The results were not experimentally validated.</li> <li>The study was conducted on rectangular cells and did not consider other geometries.</li> <li>The study did not consider the effect of the ambient temperature, discharge rate, and coolant velocity.</li> </ul>
9	Li et al. [167]	2023	Air-BTMS	Genetic Programming and Response/NSGA-II and MOGA Surface Model	$v, d_1, d_2, d_3, d_4, d_5$	Maximum temperature and cyclical cost	Higher temperature operating condition significantly decreased battery life cycle	<ul style="list-style-type: none"> <li>The study did not consider the effect of the discharge rate and pressure drop.</li> <li>The results were not experimentally validated.</li> </ul>
10	Zhang et al. [168]	2023	Liquid-BTMS	NSGA-II	$i, f, j, \beta, \theta$	$h, \Delta P$	$\Delta P$ is reduced by 64.72%, and $T_{avg}$ was decreased by 1.01% of Arcing channel	<ul style="list-style-type: none"> <li>The study was conducted on square cells and did not consider other geometries.</li> <li>The study did not consider the effects of the discharge rate.</li> </ul>
11	Fan er al. [169]	2023	Liquid-BTMS	Genetic Algorithm	Charging current trajectories	Trade-off between temperature difference and charging time	Temperature difference and charging time are decreased by 37.9% and 11.9%, respectively, using optimized charging strategy	<ul style="list-style-type: none"> <li>The study did not consider the effects of the charging rate.</li> </ul>

**Table 3.** *Cont.*

No.	Authors	Year	BTMS	AI/ML Used	Input Parameters	Goal/Target	Major Findings	Gaps
12	Fan et al. [170]	2023	Liquid–BTMS	Kriging Model/NCGA	$G, W, Re$	$T_m, T_\sigma, \Delta P$	Thermal performance of optimized MSTV was enhanced by 17.3%	<ul style="list-style-type: none"> <li>The study was conducted on prismatic-type cells and did not consider other geometries.</li> <li>The study did not consider the effect of the ambient temperature and discharge rate.</li> </ul>
13	Fan et al. [171]	2022	Air–BTMS	MOE/NSGA-II	$X1, X2, X3, Xh$	$T_m, \Delta T, \Delta P$	Optimized design decreased $T_{max}, T_d, \Delta P$ by 9%, 17.6%, and 8.9%, respectively.	<ul style="list-style-type: none"> <li>The study did not consider the effect of the ambient temperature and discharge rate.</li> </ul>
14	Çolak [172]	2022	Liquid–BTMS	Levenberg–Marquardt, Bayesian Regularization, and Scaled Conjugate Gradient	Discharge rate, flow rate, and inlet temperature	Average temperature of battery surface and maximum temperature difference	Levenberg–Marquardt has highest accuracy of prediction	<ul style="list-style-type: none"> <li>The results were not experimentally validated.</li> </ul>
15	Yalçın et al. [173]	2022	Liquid–BTMS	CNN–ABC Model	Heat generation rate and voltage variables	Heat generation rate and voltage estimations	CNN–ABC model showed best prediction compared with LR, MLR, DT, RF, SVM, LSTN, and CNN	<ul style="list-style-type: none"> <li>The study was conducted on prismatic-type cells and did not consider other geometries.</li> </ul>
16	Liao et al. [174]	2021	Air/Liquid–BTMS	RSM/NSGA-II	$W_h, W_v, D_c, D_h, D_v, T_h, H$	$T_m, \Delta T, P_{max}$	Optimized design decreased $T_m$ to 304.5, $\Delta T$ to 0.88 K, and $P_{max}$ to 710.01 Pa	<ul style="list-style-type: none"> <li>The study was conducted on prismatic-type cells and did not consider other geometries.</li> <li>The study did not consider the effect of the coolant flow rate and discharge rate.</li> </ul>
17	Chen et al. [175]	2021	Liquid–BTMS	Artificial Neural Network	$I_1, I_2, I_3, Q$	$T_m, TSD, W$	$T_m, TSD$ , and $W$ were decreased to 33.35 °C, 0.8 °C, and 0.02 J, respectively	<ul style="list-style-type: none"> <li>The study was conducted on prismatic-type cells and did not consider other geometries.</li> <li>The study did not consider the effect of the ambient temperature.</li> </ul>

**Table 3.** Cont.

No.	Authors	Year	BTMS	AI/ML Used	Input Parameters	Goal/Target	Major Findings	Gaps
18	Deng et al. [176]	2020	Liquid-BTMS	NSGA-II	D1, $\omega$ , $\gamma$ , dc, qm	$h, f$	$h$ was enhanced by 17.19% and $f$ was decreased by 85.5%	<ul style="list-style-type: none"> <li>The study was conducted on prismatic-type cells and did not consider other geometries.</li> <li>The study did not consider the effect of the ambient temperature and discharge rate.</li> </ul>
19	Garg et al. [177]	2020	Air-BTMS	ANS/NSGA II	X1, X2, X3, X4, V	V, $\Delta T$ , TSD	V, $\Delta T$ , and TSD were decreased by 29.21, 35.66%, and 78.69%, respectively	<ul style="list-style-type: none"> <li>The results were not experimentally validated.</li> <li>The study did not consider the effect of the ambient temperature and discharge rate.</li> <li>The study was conducted on prismatic-type cells and did not consider other geometries.</li> </ul>
20	Lei et al. [178]	2024	Air-BTMS	NSGA II	Coolant temperature, air flow rate, and engine speed	Engine fuel consumption and battery SOH	Fuel consumption was reduced by 4.85% and SOH was improved by 3.7%	<ul style="list-style-type: none"> <li>Only used lab-tested data, no on-road data.</li> <li>Short-term battery aging.</li> <li>Limited driving scenarios.</li> </ul>

**Table 4.** Summary table of passive BTMSs using AI and ML.

No.	Authors	Year	BTMS	AI/ML Used	Input Parameters	Goal/Target	Major Findings	Gaps
1	Amber et al. [179]	2024	PCM-BTMS	Linear Regression, Support Vector Regression (SVR), Decision Trees, and Polynomial Regression	PCM thickness, discharge rate, ambient temperature, and PCM type	Battery temperatures	Polynomial regression had a higher $R^2$ of 0.997 and a lower RSME of 0.629. Moreover, the optimal thickness was 5 mm, and the higher thermal conductivity of the inorganic types has shown better thermal performance than the organic types.	<ul style="list-style-type: none"> <li>The study focused only on the prismatic lithium-ion battery type.</li> <li>The results were not experimentally validated.</li> </ul>

**Table 4.** Cont.

No.	Authors	Year	BTMS	AI/ML Used	Input Parameters	Goal/Target	Major Findings	Gaps
2	Goud et al. [180]	2023	PCM-BTMS	Adaptive Neuro-Fuzzy Inference System	Type of cooling, battery module C-rate, and time	Maximum surface temperature of the battery	The PCM-BTMS decreased the maximum surface temperature by 31.72%, with a discharge rate of up to 5 C. The ANFIS model had higher accuracy with an R-value of 0.99.	<ul style="list-style-type: none"> <li>The study did not consider a wide range of charge rates.</li> <li>The study did not consider the influence of PCM thickness.</li> </ul>
3	Boonma et al. [181]	2022	HP-BTMS	Pattern-Based Machine Learning	Geometry of CBHP (pairs and clusters), initial battery and heat pipe conditions, temperature profiles during charge/discharge cycles, and variables affecting boiling/condensation processes	Battery temperature profiles, HP temperature, condensation ratio, thermal conductivity variations, and overall BTMS efficiency	Increasing the condensation surface area and optimizing pair/cluster configurations decreased the maximum surface temperature and the difference temperature by 27% and 13.43%, respectively.	<ul style="list-style-type: none"> <li>The result was not verified with the experimental test.</li> </ul>
4	Muthya Goud et al. [182]	2022	PCM-BTMS	Adaptive Neuro-Fuzzy Inference System	PCM type, sample heating rate, and temperature	Predicted heat flow rate of PCM	PCM-BC24, with 24% biochar and 1% MWCNT, enhanced the thermal conductivity and effusivity by 458.72% and 146.25%, respectively.	<ul style="list-style-type: none"> <li>The proposed design has not been applied to the battery pack.</li> </ul>
5	Kolodziejczyk et al. [183]	2021	PCM-BTMS	Convolutional Neural Networks	Images of CPCMs microstructures	Thermal conductivity of CPCMs and electrochemical model output heat generation rates	The proposed model had a 5% mean absolute percentage error in predicting the thermal conductivities.	<ul style="list-style-type: none"> <li>The results were not experimentally validated.</li> </ul>

**Table 5.** Summary table of hybrid BTMSs using AI and ML.

No.	Authors	Year	BTMS	AI/ML Used	Input Parameters	Goal/Target	Major Findings
1	Zhang et al. [184]	2024	PCM and air cooling with cantor fractal fin	Backpropagation (BP) neural network	SoC, n of cantor fractal fin, PCM combination, PCM proportion, air flow direction, discharge rate, ambient temperature	$T_m$ and $\Delta T_{max}$	<ul style="list-style-type: none"> <li>PCM blocks kept <math>T_{max}</math> at 308.8 K and <math>\Delta T_{max}</math> at 1.64 K under 4C discharge rate.</li> <li>Cantor fin reduced <math>T_{max}</math> by 0.53 K compared to rectangular fin.</li> <li>The BP neural network could predict the <math>T_{max}</math> and <math>\Delta T_{max}</math> within <math>\pm 10\%</math>.</li> </ul>

**Table 5.** Cont.

No.	Authors	Year	BTMS	AI/ML Used	Input Parameters	Goal/Target	Major Findings
2	Fini et al. [185]	2023	Water cooling with PCM	ANN	Re, volume fraction of microencapsulated PCM ( $\phi$ ), average temperature, temperature standard deviation	Nu and $\Delta P$	<ul style="list-style-type: none"> <li>Increasing the Reynolds number from 100 to 300 enhances the Nusselt number by up to 23% for proposed geometries, compared to just 6% for conventional channels.</li> <li>When the Reynolds number increases, the average temperature of the battery is reduced by 9%, while the temperature deviation decreases by 25%.</li> <li>The friction factor increases by 160% for the worst-performing geometry compared to the best-performing geometry, indicating a substantial difference depending on the geometry used.</li> </ul>
3	Wang et al. [186]	2023	Two-phase nanofluid with PCM	AI technique	Horizontal distance, vertical distance, nanofluid input size	Heat transfer coefficient and $T_m$	<ul style="list-style-type: none"> <li>The most significant <math>\Delta P</math> (583% difference) occurs at the highest nanofluid input, the highest horizontal distance, and the lowest vertical distance between batteries.</li> <li>The lowest <math>\Delta T_{max}</math> (7.15 °C difference) was obtained with the lowest horizontal and vertical distances and the smallest nanofluid input size.</li> <li>The maximum heat transfer coefficient, 794.26 W/m<sup>2</sup>K, was observed at the highest horizontal distance, lowest vertical distance, and highest nanofluid input.</li> </ul>

**Table 5.** Cont.

No.	Authors	Year	BTMS	AI/ML Used	Input Parameters	Goal/Target	Major Findings
4	Xie et al. [187]	2024	Liquid cooling with PCM	Random forest (RF), neural networks (NNs), and gradient boosting (GB).	Battery arrangement structure (e.g., single row or double row), liquid flow direction (e.g., upper nozzle inflow, staggered inflow), mass flow rate, liquid cooling startup temperature, PCM melting point, discharge rate (3C or 5C), initial battery temperature	$T_m$ , $\Delta T_{max}$ , and energy consumption	<ul style="list-style-type: none"> <li>The hybrid PCM liquid cooling system reduced <math>T_{max}</math> by 15.18 °C and 27.5 °C during 3C and 5C discharge compared to systems without liquid cooling.</li> <li>The optimization for the cooling flow rate reduced energy consumption by 94.71% during 5C discharge.</li> <li>The RF model predicted the system's performance with errors below 5%, closely matching CFD results.</li> </ul>
5	Chen et al. [188]	2022	Liquid cooling with PCM	ANN	Charging current rate (2C, 2.5C, and 3C), mass flow rate, PCM thickness	$T_m$ and temperature standard deviation (TSD)	<ul style="list-style-type: none"> <li>The regression accuracy was 99.942% for <math>T_{max}</math> and 99.507% for TSD.</li> <li>The variation between the predicted and experimental data was minimal, proving the ANN model's accuracy in predicting thermal performance.</li> </ul>
6	Liu et al. [189]	2022	Airflow with PCM	ANN		Battery temperature and $\Delta P$	<ul style="list-style-type: none"> <li>Smaller PCM compartments result in faster freezing of PCM and lower average battery temperatures.</li> <li>Increasing the PCM compartment increases maximum and average battery temperatures.</li> <li>The ANN predictions were highly accurate, with less than 3% error, effectively simulating thermal behavior and energy usage in the system.</li> </ul>

**Table 5.** Cont.

No.	Authors	Year	BTMS	AI/ML Used	Input Parameters	Goal/Target	Major Findings
7	Alqaed et al. [190]	2024	Air cooling with PCM	ANN	Battery pack arrangement, airflow velocity, PCM properties, temperature change over 2500 s	$T_m$	<ul style="list-style-type: none"> <li>The square configuration of batteries, combined with curved blades, was the most effective for reducing temperature, with a reduction of up to 10 °C compared to the diamond arrangement.</li> <li>The mean squared error (MSE) obtained was 0.0972 with a 2.01% error.</li> </ul>
8	Yang et al. [191]	2021	Bionic liquid mini-channel in cooling plate with PCM	Back propagation (BP) neural network	Ambient temperature, $T_m$ , $\Delta T_{\max}$ , discharge current, cycle conditions	Inlet flow rate	<ul style="list-style-type: none"> <li>The honeycomb-like design with a hexagonal cooling plate minimizes maximum temperature, temperature difference, and pressure loss when compared to typical rectangular cooling plates.</li> <li>The optimal performance was obtained with an inlet flow rate of <math>0.001 \text{ kg} \cdot \text{s}^{-1}</math>, a channel width of 2.5 mm, and two tube junctions.</li> <li>The BP model successfully stabilizes the battery module's temperature at 312 K with a temperature variation of 3.5 K under various situations.</li> </ul>

## 5. Discussion

In this study, a comprehensive investigation of recent research on BTMSs—including active, passive, and hybrid systems—utilized AI and ML techniques for optimizing the performance of BTMSs, particularly in managing crucial parameters such as maximum temperature, temperature difference, and pressure drop. Current research highlights the effectiveness of ML algorithms for predicting and controlling temperature variations, achieving temperature uniformity, and reducing energy consumption within LIBs. Several ML models and input parameters are discussed, demonstrating promising results in system efficiency. However, the review identifies persisting challenges, such as unconsidered variables in experimental work. The following is a summary of the main findings of this review:

- The active cooling, including air-BTMS and liquid-BTMS using AI and ML, has shown superior thermal behavior. Both reduced the maximum surface temperature, enhanced the homogeneity of the temperature inside the battery pack, and reduced energy consumption by optimizing the dimensions of the cooling system, coolant flow rate, and discharge rate. One of the significant multi-objective optimization methods that has been intensively used is NSGA-II, with a higher  $R^2$  value of up to 0.99. Moreover, genetic algorithms, Kriging models, and artificial neural networks are frequently utilized in numerous studies due to their high efficiency in handling nonlinear relationships between variables and their reduced computational time requirements. On the other hand, there are still limitations with active cooling using AI and ML, such as the need to optimize the effect of the nanofluid on the battery pack. It is well known that working fluid plays a key role in influencing the ion thermal behavior of the battery. Furthermore, most of the studies had challenges with validating the results with experimental tests; numerous studies have been conducted on the specified type of battery cells. In addition, there is a vital need to observe and study the health monitoring of the battery (SoH). Also, most investigations have studied and optimized the BTMS with a constant ambient temperature and constant discharge/charging rate.
- Passive cooling, including PCM-BTMS and HP-BTMS using AI and ML, has shown more significant potential to enhance uniformity and reduce the battery's surface temperature. As a result, most of the proposed predictive models (SVR, ANFIS, and CNN) had an  $R^2$  value of up to 0.99, and the maximum surface temperature reduction was 31.72%; in addition, the thickness of the PCM had a significant influence on the thermal performance of the PCM-BTMS. However, due to their lower thermal conductivity, the PCM-BTMS still struggled with maintaining the temperature in the optimal operating range. Furthermore, the PCM-BTMS relies on mass, resulting in bulky and heavy systems. On the other hand, there is still a limitation of passive BTMSs, such as the HP-BTMS using AI and ML, which has not been intensively investigated. Moreover, the PCM-BTMS using AI and ML has not been studied and verified with experimental tests, especially for the operating cycle (while driving) compared with charging and discharging cycles. Furthermore, the nano PCM-BTMS should be considered in future work.
- According to the literature for hybrid BTMSs with AI/ML, they have demonstrated significant success in improving cooling efficiency, energy consumption, and thermal stability in LIBs. Multi-objective optimization approaches like NSGA-II have provided balanced cooling performance and minimum pressure drops, resulting in optimal flow rates and channel designs. ANN models have allowed for more accurate temperature predictions in PCM-enhanced BTMS settings, greatly lowering temperature variance. Furthermore, models such as backpropagation neural networks (BPNNs)

and LSTM have been utilized to anticipate temperature distribution and manage system responses, resulting in high prediction accuracy and enhanced thermal uniformity while using less energy. However, limitations remain, since many models are designed for specific situations, and expansion to other battery applications remains difficult. Further study might extend these methodologies to cover a broader range of configurations, materials, and operating conditions for hybrid BTMS optimization. Furthermore, extra LIB parameters, such as SoH and internal resistance increase, must be investigated. Additionally, more experimental work is needed to simulate actual situations for BTMSs.

- AI and ML can significantly enhance BTMSs by enabling real-time thermal prediction, adaptive cooling control, and degradation mitigation, thereby extending battery lifespan and maintaining optimal operating conditions (15–35 °C). AI and ML offer substantial advantages, including high-accuracy temperature prediction ( $R^2 = 0.99$  for ANN), optimized cooling efficiency, and adaptive control strategies that enhance safety and prolong battery lifespan. Techniques such as ANN, LSTM, and reinforcement learning enable real-time thermal monitoring, as well as a reduction in maximum temperatures and temperature differences, ensuring a homogeneous thermal distribution inside the battery system. AI-driven multi-objective optimization, such as NSGA II, MOGA, and NCGA models, also improves energy efficiency by significantly lowering cooling demands by reducing the pressure drop, heat transfer coefficient, and power consumption. However, these methods present notable challenges, including high computational costs, complex model development, and a heavy reliance on extensive, high-quality training datasets. Scalability remains a concern, particularly when transitioning from lab-scale models to real-world battery packs, where diverse operating conditions and pack configurations complicate implementation. Additionally, deep learning approaches, while powerful, encountered issues like overfitting require significant expertise for fine-tuning. Hybrid approaches that integrate experimental-based data and CFD-based data with AI/ML show promise in balancing accuracy with practicality, offering a viable path forward for robust and efficient BTMSs.

## 6. Conclusions and Future Work

This study reviewed a comprehensive investigation of BTMS developments by integrating AI and ML approaches. Recent developments in AI and ML across a wide range of applications have created new opportunities for improving BTMS performance in temperature control, energy efficiency, and lifecycle management.

Various types of BTMSs, including active, passive, and hybrid systems utilizing AI and ML, have shown significant potential in optimizing system parameters, reducing maximum surface temperatures, and optimizing energy consumption. This is primarily attributed to the efficiency of algorithms such as NSGA-II and ANN, which manage complex, nonlinear relationships effectively. Furthermore, the predictive accuracy of models such as the CNN and ANFIS is remarkable, although challenges remain in integrating these models with experimental results and extending studies beyond charging/discharging cycles. The study demonstrates the potential role of AI and ML within BTMSs while illustrating current obstacles, such as the need for comprehensive validation using experimental data and the incorporation of real-time operational variables like ambient temperature changes, SoC, and SoH. Furthermore, the complexity of real-world driving conditions continues to present challenges in deploying these advanced approaches.

As a result, several potential directions for future research can be stated as follows:

- Establish extensive experimental setups that simulate real BTMS operational situations to optimize model outputs, improve system design, and include realistic scenarios for the experimental study, such as charging and discharging rates.
- Extending the study to include additional variables such as SoH and internal resistance increase in LIBs to better understand how AI/ML affects battery longevity and performance.
- Extending studies beyond specific cell types or configurations to evaluate the flexibility and adaptiveness of AI/ML applications across an extensive range of battery technologies.
- Intensify research on nanofluid and nanocomposite PCMs to improve the thermal performance of BTMSs and integrate this technology with the input parameters to AI/ML.

Consequently, future research can focus on these issues and establish AI and ML as critical components in expanding BTMS technology and ensuring efficient, dependable, and long-term battery management solutions.

**Author Contributions:** Conceptualization, A.A. and A.S.; methodology, A.A. and A.S.; writing—original draft preparation, A.A. and A.S.; writing—review and editing, A.A. and A.S.; visualization, A.A. and A.S.; supervision, M.H.S. and M.A.J.; project administration, M.H.S. and M.A.J.; funding acquisition, M.H.S. and M.A.J. All authors have read and agreed to the published version of the manuscript.

**Funding:** The authors would like to thank the Natural Sciences and Engineering Research Council of Canada (NSERC grant #401366) for the funding support provided for this research.

**Conflicts of Interest:** The authors declare no conflict of interest.

## Abbreviations

AI	Artificial Intelligence
ANN	Artificial Neural Network
BEV	Battery Electric Vehicle
BTMS	Battery Thermal Management System
CFD	Computational Fluid Dynamics
COP	Coefficient of Performance
CNN	Convolutional Neural Network
DCIR	Direct Current Internal Resistance
EV	Electric Vehicle
GHG	Greenhouse Gas
HEV	Hybrid Electric Vehicle
HP	Heat Pipe
HPACS	Heat Pump Air Conditioning System
ICE	Internal Combustion Engine
LCP	Liquid Cold Plate
LIB	Lithium-Ion Battery
LSTM	Long Short-Term Memory
ML	Machine Learning
MOGA	Multi-Objective Genetic Algorithm
NSGA-II	Non-Dominated Sorting Genetic Algorithm II
PCM	Phase-Change Material
PHEV	Plug-in Hybrid Electric Vehicle
PSO	Particle Swarm Optimization
RF	Random Forest
RSM	Response Surface Methodology
SEI	Solid-Electrolyte Interface

SoC	State of Charge
SoH	State of Health
SVR	Support Vector Regression
TEC	Thermoelectric Cooler
TR	Thermal Runaway
XGB	X-Gradient Boosting

**Nomenclature:**

I	Current
$\dot{Q}$	Heat Generation
$R_i$	Internal Resistance
T	Battery Temperature
$T_m$	Maximum Temperature
$\Delta T$	Temperature Difference
$V_o$	Open Circuit Voltage
V	Nominal Voltage

## References

1. Morfeldt, J.; Davidsson Kurland, S.; Johansson, D.J.A. Carbon Footprint Impacts of Banning Cars with Internal Combustion Engines. *Transp. Res. D Transp. Environ.* **2021**, *95*, 102807. [[CrossRef](#)]
2. Leach, F.; Kalghatgi, G.; Stone, R.; Miles, P. The Scope for Improving the Efficiency and Environmental Impact of Internal Combustion Engines. *Transp. Eng.* **2020**, *1*, 100005. [[CrossRef](#)]
3. Zhao, X.; Hu, H.; Yuan, H.; Chu, X. How Does Adoption of Electric Vehicles Reduce Carbon Emissions? Evidence from China. *Heliyon* **2023**, *9*, e20296. [[CrossRef](#)] [[PubMed](#)]
4. Veza, I.; Asy'ari, M.Z.; Idris, M.; Epin, V.; Rizwanul Fattah, I.M.; Spraggon, M. Electric Vehicle (EV) and Driving towards Sustainability: Comparison between EV, HEV, PHEV, and ICE Vehicles to Achieve Net Zero Emissions by 2050 from EV. *Alex. Eng. J.* **2023**, *82*, 459–467. [[CrossRef](#)]
5. Dobó, Z.; Dinh, T.; Kulcsár, T. A Review on Recycling of Spent Lithium-Ion Batteries. *Energy Rep.* **2023**, *9*, 6362–6395. [[CrossRef](#)]
6. Sasaki, T.; Ukyo, Y.; Novák, P. Memory Effect in a Lithium-Ion Battery. *Nat. Mater.* **2013**, *12*, 569–575. [[CrossRef](#)] [[PubMed](#)]
7. Kumar, S.; Singh, V.; Goel, R. Strategic Forecasting for Electric Vehicle Sales: A Cutting Edge Holistic Model Leveraging Key Factors and Machine Learning Technique. *Transp. Dev. Econ.* **2024**, *10*, 23. [[CrossRef](#)]
8. Ali, H.M. Thermal Management Systems for Batteries in Electric Vehicles: A Recent Review. *Energy Rep.* **2023**, *9*, 5545–5564. [[CrossRef](#)]
9. Zou, B.; Zhang, L.; Xue, X.; Tan, R.; Jiang, P.; Ma, B.; Song, Z.; Hua, W. A Review on the Fault and Defect Diagnosis of Lithium-Ion Battery for Electric Vehicles. *Energies* **2023**, *16*, 5507. [[CrossRef](#)]
10. Shen, D.; Lyu, C.; Yang, D.; Hinds, G.; Ma, K.; Xu, S.; Bai, M. Concurrent Multi-Fault Diagnosis of Lithium-Ion Battery Packs Using Random Convolution Kernel Transformation and Gaussian Process Classifier. *Energy* **2024**, *306*, 132467. [[CrossRef](#)]
11. Amba Prasad Rao, G.; Shravan Kumar, S.R. A Review of Integrated Battery Thermal Management Systems for Lithium-Ion Batteries of Electric Vehicles. *E-Prime—Adv. Electr. Eng. Electron. Energy* **2024**, *8*, 100526. [[CrossRef](#)]
12. Al Miaari, A.; Ali, H.M. Batteries Temperature Prediction and Thermal Management Using Machine Learning: An Overview. *Energy Rep.* **2023**, *10*, 2277–2305. [[CrossRef](#)]
13. Ma, S.; Jiang, M.; Tao, P.; Song, C.; Wu, J.; Wang, J.; Deng, T.; Shang, W. Temperature Effect and Thermal Impact in Lithium-Ion Batteries: A Review. *Prog. Nat. Sci. Mater. Int.* **2018**, *28*, 653–666. [[CrossRef](#)]
14. Chen, Y.; Kang, Y.; Zhao, Y.; Wang, L.; Liu, J.; Li, Y.; Liang, Z.; He, X.; Li, X.; Tavajohi, N.; et al. A Review of Lithium-Ion Battery Safety Concerns: The Issues, Strategies, and Testing Standards. *J. Energy Chem.* **2021**, *59*, 83–99. [[CrossRef](#)]
15. Alipour, M.; Ziebert, C.; Conte, F.V.; Kizilel, R. A Review on Temperature-Dependent Electrochemical Properties, Aging, and Performance of Lithium-Ion Cells. *Batteries* **2020**, *6*, 35. [[CrossRef](#)]
16. Thomas, E.V.; Case, H.L.; Doughty, D.H.; Jungst, R.G.; Nagasubramanian, G.; Roth, E.P. Accelerated Power Degradation of Li-Ion Cells. *J. Power Sources* **2003**, *124*, 254–260. [[CrossRef](#)]
17. Bandhauer, T.M.; Garimella, S.; Fuller, T.F. Temperature-Dependent Electrochemical Heat Generation in a Commercial Lithium-Ion Battery. *J. Power Sources* **2014**, *247*, 618–628. [[CrossRef](#)]
18. Saeed, A.; Alshehri, A.; Munteshari, O. Calendar Aging of Commercial Lithium Ion Batteries under Realistic Conditions. *Therm. Sci. Eng. Prog.* **2024**, *49*, 102436. [[CrossRef](#)]
19. Gao, T.; Bai, J.; Ouyang, D.; Wang, Z.; Bai, W.; Mao, N.; Zhu, Y. Effect of Aging Temperature on Thermal Stability of Lithium-Ion Batteries: Part A—High-Temperature Aging. *Renew. Energy* **2023**, *203*, 592–600. [[CrossRef](#)]

20. Chen, S.; Wei, X.; Zhang, G.; Wang, X.; Zhu, J.; Feng, X.; Dai, H.; Ouyang, M. All-Temperature Area Battery Application Mechanism, Performance, and Strategies. *Innovation* **2023**, *4*, 100465. [[CrossRef](#)] [[PubMed](#)]
21. Luo, H.; Wang, Y.; Feng, Y.H.; Fan, X.Y.; Han, X.; Wang, P.F. Lithium-Ion Batteries under Low-Temperature Environment: Challenges and Prospects. *Materials* **2022**, *15*, 8166. [[CrossRef](#)] [[PubMed](#)]
22. Kong, D.; Zhao, H.; Ping, P.; Zhang, Y.; Wang, G. Effect of Low Temperature on Thermal Runaway and Fire Behaviors of 18650 Lithium-Ion Battery: A Comprehensive Experimental Study. *Process Saf. Environ. Prot.* **2023**, *174*, 448–459. [[CrossRef](#)]
23. Smart, M.C.; Ratnakumar, B.V.; Whitcanack, L.D.; Chin, K.B.; Surampudi, S.; Croft, H.; Tice, D.; Staniewicz, R. Improved Low-Temperature Performance of Lithium-Ion Cells with Quaternary Carbonate-Based Electrolytes. *J. Power Sources* **2003**, *119–121*, 349–358. [[CrossRef](#)]
24. Gharehghani, A.; Rabiei, M.; Mehranfar, S.; Saeedipour, S.; Mahmoudzadeh Andwari, A.; García, A.; Reche, C.M. Progress in Battery Thermal Management Systems Technologies for Electric Vehicles. *Renew. Sustain. Energy Rev.* **2024**, *202*, 114654. [[CrossRef](#)]
25. Fan, L.; Khodadadi, J.M.; Pesaran, A.A. A Parametric Study on Thermal Management of an Air-Cooled Lithium-Ion Battery Module for Plug-in Hybrid Electric Vehicles. *J. Power Sources* **2013**, *238*, 301–312. [[CrossRef](#)]
26. Hossain, M.H.; Chowdhury, M.A.; Hossain, N.; Islam, M.A.; Mobarak, M.H. Advances of Lithium-Ion Batteries Anode Materials—A Review. *Chem. Eng. J. Adv.* **2023**, *16*, 100569. [[CrossRef](#)]
27. Rojas, O.E.; Khan, M.A. A Review on Electrical and Mechanical Performance Parameters in Lithium-Ion Battery Packs. *J. Clean. Prod.* **2022**, *378*, 134381. [[CrossRef](#)]
28. Amer, M.; Masri, J.; Dababat, A.; Sajjad, U.; Hamid, K. Electric Vehicles: Battery Technologies, Charging Standards, AI Communications, Challenges, and Future Directions. *Energy Convers. Manag. X* **2024**, *24*, 100751. [[CrossRef](#)]
29. Borah, R.; Hughson, F.R.; Johnston, J.; Nann, T. On Battery Materials and Methods. *Mater. Today Adv.* **2020**, *6*, 100046. [[CrossRef](#)]
30. Gao, Y.; Pan, Z.; Sun, J.; Liu, Z.; Wang, J. High-Energy Batteries: Beyond Lithium-Ion and Their Long Road to Commercialisation. *Nano-Micro Lett.* **2022**, *14*, 94. [[CrossRef](#)] [[PubMed](#)]
31. Wang, L.; Jin, M.; Cai, Y.; Lian, Y.; Zhao, X.; Wang, R.; Qiao, S.; Chen, L.; Yan, X. Construction of Electrochemical Model for High C-Rate Conditions in Lithium-Ion Battery Based on Experimental Analogy Method. *Energy* **2023**, *279*, 128073. [[CrossRef](#)]
32. Gao, Z.; Xie, H.; Yang, X.; Niu, W.; Li, S.; Chen, S. The Dilemma of C-Rate and Cycle Life for Lithium-Ion Batteries under Low Temperature Fast Charging. *Batteries* **2022**, *8*, 234. [[CrossRef](#)]
33. Wu, C.; Sun, Y.; Tang, H.; Zhang, S.; Yuan, W.; Zhu, L.; Tang, Y. A Review on the Liquid Cooling Thermal Management System of Lithium-Ion Batteries. *Appl. Energy* **2024**, *375*, 124173. [[CrossRef](#)]
34. Yang, L.; Liu, F.; Li, F.; Chen, Z.; Wang, J.; Gao, L.; Xiao, F.; Sun, J.; Romagnoli, A. Thermal Runaway Prevention and Mitigation for Lithium-Ion Battery-Powered Electric Aircraft: Challenges and Perspectives. *Aerosop. Traffic Saf.* **2024**, *1*, 103–118. [[CrossRef](#)]
35. Ren, Z.; Du, C.; Wu, Z.; Shao, J.; Deng, W. A Comparative Study of the Influence of Different Open Circuit Voltage Tests on Model-Based State of Charge Estimation for Lithium-Ion Batteries. *Int. J. Energy Res.* **2021**, *45*, 13692–13711. [[CrossRef](#)]
36. Suganya, R.; Joseph, L.M.I.L.; Kollem, S. Understanding Lithium-Ion Battery Management Systems in Electric Vehicles: Environmental and Health Impacts, Comparative Study, and Future Trends: A Review. *Results Eng.* **2024**, *24*, 103047. [[CrossRef](#)]
37. Chen, L.; Zhang, M.; Ding, Y.; Wu, S.; Li, Y.; Liang, G.; Li, H.; Pan, H. Estimation the Internal Resistance of Lithium-Ion-Battery Using a Multi-Factor Dynamic Internal Resistance Model with an Error Compensation Strategy. *Energy Rep.* **2021**, *7*, 3050–3059. [[CrossRef](#)]
38. Heiskanen, S.K.; Kim, J.; Lucht, B.L. Generation and Evolution of the Solid Electrolyte Interphase of Lithium-Ion Batteries. *Joule* **2019**, *3*, 2322–2333. [[CrossRef](#)]
39. Zimmerman, A.H. Self-Discharge Losses in Lithium-Ion Cells. *IEEE Aerosp. Electron. Syst. Mag.* **2004**, *2*, 19–24. [[CrossRef](#)]
40. Birk, C.R.; Roberts, M.R.; McTurk, E.; Bruce, P.G.; Howey, D.A. Degradation Diagnostics for Lithium Ion Cells. *J. Power Sources* **2017**, *341*, 373–386. [[CrossRef](#)]
41. Wang, Y.; Liu, B.; Han, P.; Hao, C.; Li, S.; You, Z.; Wang, M. Optimization of an Air-Based Thermal Management System for Lithium-Ion Battery Packs. *J. Energy Storage* **2021**, *44*, 103314. [[CrossRef](#)]
42. Wang, A.; Kadam, S.; Li, H.; Shi, S.; Qi, Y. Review on Modeling of the Anode Solid Electrolyte Interphase (SEI) for Lithium-Ion Batteries. *NPJ Comput. Mater.* **2018**, *4*, 15. [[CrossRef](#)]
43. Meister, P.; Jia, H.; Li, J.; Kloepsch, R.; Winter, M.; Placke, T. Best Practice: Performance and Cost Evaluation of Lithium Ion Battery Active Materials with Special Emphasis on Energy Efficiency. *Chem. Mater.* **2016**, *28*, 7203–7217. [[CrossRef](#)]
44. Zhang, X.; Li, Z.; Luo, L.; Fan, Y.; Du, Z. A Review on Thermal Management of Lithium-Ion Batteries for Electric Vehicles. *Energy* **2022**, *238*, 121652. [[CrossRef](#)]
45. Jaguemont, J.; Boulon, L.; Dube, Y.; Martel, F. Thermal Management of a Hybrid Electric Vehicle in Cold Weather. *IEEE Trans. Energy Convers.* **2016**, *31*, 1110–1120. [[CrossRef](#)]
46. Wu, W.; Wang, S.; Wu, W.; Chen, K.; Hong, S.; Lai, Y. A Critical Review of Battery Thermal Performance and Liquid Based Battery Thermal Management. *Energy Convers. Manag.* **2019**, *182*, 262–281. [[CrossRef](#)]

47. Tete, P.R.; Gupta, M.M.; Joshi, S.S. Developments in Battery Thermal Management Systems for Electric Vehicles: A Technical Review. *J. Energy Storage* **2021**, *35*, 102255. [[CrossRef](#)]
48. Bernardi, D.; Pawlikowski, E.; Newman, J. A General Energy Balance for Battery Systems. *J. Electrochemical Society* **1985**, *132*, 5. [[CrossRef](#)]
49. Hwang, F.S.; Confrey, T.; Reidy, C.; Picovici, D.; Callaghan, D.; Culliton, D.; Nolan, C. Review of Battery Thermal Management Systems in Electric Vehicles. *Renew. Sustain. Energy Rev.* **2024**, *192*, 114171. [[CrossRef](#)]
50. Sheng, L.; Su, L.; Zhang, H.; Li, K.; Fang, Y.; Ye, W.; Fang, Y. Numerical Investigation on a Lithium Ion Battery Thermal Management Utilizing a Serpentine-Channel Liquid Cooling Plate Exchanger. *Int. J. Heat Mass Transf.* **2019**, *141*, 658–668. [[CrossRef](#)]
51. Wang, Y.; Xu, X.; Liu, Z.; Kong, J.; Zhai, Q.; Zakaria, H.; Wang, Q.; Zhou, F.; Wei, H. Optimization of Liquid Cooling for Prismatic Battery with Novel Cold Plate Based on Butterfly-Shaped Channel. *J. Energy Storage* **2023**, *73*, 109161. [[CrossRef](#)]
52. Wang, Q.; Jiang, B.; Li, B.; Yan, Y. A Critical Review of Thermal Management Models and Solutions of Lithium-Ion Batteries for the Development of Pure Electric Vehicles. *Renew. Sustain. Energy Rev.* **2016**, *64*, 106–128. [[CrossRef](#)]
53. Kim, J.; Oh, J.; Lee, H. Review on Battery Thermal Management System for Electric Vehicles. *Appl. Therm. Eng.* **2019**, *149*, 192–212. [[CrossRef](#)]
54. Gozdur, R.; Guzowski, B.; Dimitrova, Z.; Noury, A.; Mitukiewicz, G.; Batory, D. An Energy Balance Evaluation in Lithium-Ion Battery Module under High Temperature Operation. *Energy Convers. Manag.* **2021**, *227*, 113565. [[CrossRef](#)]
55. Liao, C.; Wang, W.; Wang, J.; Han, L.; Qiu, S.; Song, L.; Gui, Z.; Kan, Y.; Hu, Y. Magnetron Sputtering Deposition of Silicon Nitride on Polyimide Separator for High-Temperature Lithium-Ion Batteries. *J. Energy Chem.* **2021**, *56*, 1–10. [[CrossRef](#)]
56. Ma, Z.; Chen, J.; Vatamanu, J.; Borodin, O.; Bedrov, D.; Zhou, X.; Zhang, W.; Li, W.; Xu, K.; Xing, L. Expanding the Low-Temperature and High-Voltage Limits of Aqueous Lithium-Ion Battery. *Energy Storage Mater.* **2022**, *45*, 903–910. [[CrossRef](#)]
57. Zhang, S.S.; Xu, K.; Jow, T.R. The Low Temperature Performance of Li-Ion Batteries. *J. Power Sources* **2003**, *115*, 137–140. [[CrossRef](#)]
58. Akbarzadeh, M.; Kalogiannis, T.; Jaguemont, J.; Jin, L.; Behi, H.; Karimi, D.; Beheshti, H.; Van Mierlo, J.; Berecibar, M. A Comparative Study between Air Cooling and Liquid Cooling Thermal Management Systems for a High-Energy Lithium-Ion Battery Module. *Appl. Therm. Eng.* **2021**, *198*, 117503. [[CrossRef](#)]
59. Deng, Y.; Feng, C.; E, J.; Zhu, H.; Chen, J.; Wen, M.; Yin, H. Effects of Different Coolants and Cooling Strategies on the Cooling Performance of the Power Lithium Ion Battery System: A Review. *Appl. Therm. Eng.* **2018**, *142*, 10–29. [[CrossRef](#)]
60. Yang, Y.; Li, W.; Xu, X.; Tong, G. Heat Dissipation Analysis of Different Flow Path for Parallel Liquid Cooling Battery Thermal Management System. *Int. J. Energy Res.* **2020**, *44*, 5165–5176. [[CrossRef](#)]
61. Zhang, C.-W.; Xu, K.-J.; Li, L.-Y.; Yang, M.-Z.; Gao, H.-B.; Chen, S.-R. Study on a Battery Thermal Management System Based on a Thermoelectric Effect. *Energies* **2018**, *11*, 279. [[CrossRef](#)]
62. Zhao, J.; Feng, X.; Tran, M.-K.; Fowler, M.; Ouyang, M.; Burke, A.F. Battery Safety: Fault Diagnosis from Laboratory to Real World. *J. Power Sources* **2024**, *598*, 234111. [[CrossRef](#)]
63. Zhao, J.; Feng, X.; Pang, Q.; Fowler, M.; Lian, Y.; Ouyang, M.; Burke, A.F. Battery Safety: Machine Learning-Based Prognostics. *Prog. Energy Combust. Sci.* **2024**, *102*, 101142. [[CrossRef](#)]
64. Mahamud, R.; Park, C. Reciprocating Air Flow for Li-Ion Battery Thermal Management to Improve Temperature Uniformity. *J. Power Sources* **2011**, *196*, 5685–5696. [[CrossRef](#)]
65. Wang, T.; Tseng, K.J.; Zhao, J.; Wei, Z. Thermal Investigation of Lithium-Ion Battery Module with Different Cell Arrangement Structures and Forced Air-Cooling Strategies. *Appl. Energy* **2014**, *134*, 229–238. [[CrossRef](#)]
66. Chen, K.; Song, M.; Wei, W.; Wang, S. Structure Optimization of Parallel Air-Cooled Battery Thermal Management System with U-Type Flow for Cooling Efficiency Improvement. *Energy* **2018**, *145*, 603–613. [[CrossRef](#)]
67. Wang, Y.-W.; Jiang, J.-M.; Chung, Y.-H.; Chen, W.-C.; Shu, C.-M. Forced-Air Cooling System for Large-Scale Lithium-Ion Battery Modules during Charge and Discharge Processes. *J. Therm. Anal. Calorim.* **2019**, *135*, 2891–2901. [[CrossRef](#)]
68. Gocmen, S.; Cetkin, E. Emergence of Elevated Battery Positioning in Air Cooled Battery Packs for Temperature Uniformity in Ultra-Fast Dis/Charging Applications. *J. Energy Storage* **2022**, *45*, 103516. [[CrossRef](#)]
69. Lazim, A.A.; Ismael, M.A. Cooling of Lithium-Ion Battery Pack Using Different Configurations of Flexible Baffled Channels. *Heat Transf.* **2024**, *53*, 1267–1291. [[CrossRef](#)]
70. Zhao, Y.; Zhang, X.; Yang, B.; Cai, S. A Review of Battery Thermal Management Systems Using Liquid Cooling and PCM. *J. Energy Storage* **2024**, *76*, 109836. [[CrossRef](#)]
71. Jithin, K.V.; Rajesh, P.K. Numerical Analysis of Single-Phase Liquid Immersion Cooling for Lithium-Ion Battery Thermal Management Using Different Dielectric Fluids. *Int. J. Heat Mass Transf.* **2022**, *188*, 122608. [[CrossRef](#)]
72. Tan, X.; Lyu, P.; Fan, Y.; Rao, J.; Ouyang, K. Numerical Investigation of the Direct Liquid Cooling of a Fast-Charging Lithium-Ion Battery Pack in Hydrofluoroether. *Appl. Therm. Eng.* **2021**, *196*, 117279. [[CrossRef](#)]
73. Wu, S.; Lao, L.; Wu, L.; Liu, L.; Lin, C.; Zhang, Q. Effect Analysis on Integration Efficiency and Safety Performance of a Battery Thermal Management System Based on Direct Contact Liquid Cooling. *Appl. Therm. Eng.* **2022**, *201*, 117788. [[CrossRef](#)]

74. Larrañaga-Ezeiza, M.; Vertiz, G.; Arroabe, P.F.; Martínez-Agirre, M.; Berasategi, J. A Novel Direct Liquid Cooling Strategy for Electric Vehicles Focused on Pouch Type Battery Cells. *Appl. Therm. Eng.* **2022**, *216*, 118869. [[CrossRef](#)]
75. Giannicchele, L.; D’Alessandro, V.; Falone, M.; Ricci, R. Experimental Study of a Direct Immersion Liquid Cooling of a Li-Ion Battery for Electric Vehicles Applications. *Int. J. Heat Technol.* **2022**, *40*, 1–8. [[CrossRef](#)]
76. Guo, Z.; Xu, J.; Xu, Z.; Mubashir, M.; Wang, H.; Mei, X. A Lightweight Multichannel Direct Contact Liquid-Cooling System and Its Optimization for Lithium-Ion Batteries. *IEEE Trans. Transp. Electrif.* **2022**, *8*, 2334–2345. [[CrossRef](#)]
77. Li, Y.; Zhou, Z.; Su, L.; Bai, M.; Gao, L.; Li, Y.; Liu, X.; Li, Y.; Song, Y. Numerical Simulations for Indirect and Direct Cooling of 54 V LiFePO<sub>4</sub> Battery Pack. *Energies* **2022**, *15*, 4581. [[CrossRef](#)]
78. Han, J.-W.; Garud, K.S.; Hwang, S.G.; Lee, M.-Y. Experimental Study on Dielectric Fluid Immersion Cooling for Thermal Management of Lithium-Ion Battery. *Symmetry* **2022**, *14*, 2126. [[CrossRef](#)]
79. Wang, Y.; Li, C.; Wen, X.; Cai, W.; Jiang, Y.; Wen, C.; Wang, Y.; Hu, L.; Yu, H.; Zhu, H.; et al. Experimental Studies on Two-Phase Immersion Liquid Cooling for Li-Ion Battery Thermal Management. *J. Energy Storage* **2023**, *72*, 108748. [[CrossRef](#)]
80. Xu, X.; Tong, G.; Li, R. Numerical Study and Optimizing on Cold Plate Splitter for Lithium Battery Thermal Management System. *Appl. Therm. Eng.* **2020**, *167*, 114787. [[CrossRef](#)]
81. Wang, G.; Gao, Q.; Yan, Y.; Wang, Y. Thermal Management Optimization of a Lithium-Ion Battery Module with Graphite Sheet Fins and Liquid Cold Plates. *Automot. Innov.* **2020**, *3*, 336–346. [[CrossRef](#)]
82. Rabiei, M.; Gharehghani, A.; Andwari, A.M. Enhancement of Battery Thermal Management System Using a Novel Structure of Hybrid Liquid Cold Plate. *Appl. Therm. Eng.* **2023**, *232*, 121051. [[CrossRef](#)]
83. Fan, L.; Li, J.; Chen, Y.; Zhou, D.; Jiang, Z.; Sun, J. Study on the Cooling Performance of a New Secondary Flow Serpentine Liquid Cooling Plate Used for Lithium Battery Thermal Management. *Int. J. Heat Mass Transf.* **2024**, *218*, 124711. [[CrossRef](#)]
84. Wei, L.; Zou, Y.; Cao, F.; Ma, Z.; Lu, Z.; Jin, L. An Optimization Study on the Operating Parameters of Liquid Cold Plate for Battery Thermal Management of Electric Vehicles. *Energies* **2022**, *15*, 9180. [[CrossRef](#)]
85. Sheng, L.; Zhang, H.; Su, L.; Zhang, Z.; Zhang, H.; Li, K.; Fang, Y.; Ye, W. Effect Analysis on Thermal Profile Management of a Cylindrical Lithium-Ion Battery Utilizing a Cellular Liquid Cooling Jacket. *Energy* **2021**, *220*, 119725. [[CrossRef](#)]
86. Zhou, H.; Zhou, F.; Zhang, Q.; Wang, Q.; Song, Z. Thermal Management of Cylindrical Lithium-Ion Battery Based on a Liquid Cooling Method with Half-Helical Duct. *Appl. Therm. Eng.* **2019**, *162*, 114257. [[CrossRef](#)]
87. Li, P.; Zhao, J.; Zhou, S.; Duan, J.; Li, X.; Zhang, H.; Yuan, J. Design and Optimization of a Liquid Cooling Thermal Management System with Flow Distributors and Spiral Channel Cooling Plates for Lithium-Ion Batteries. *Energies* **2023**, *16*, 2196. [[CrossRef](#)]
88. Sun, Y.; Bai, R.; Ma, J. Development and Analysis of a New Cylindrical Lithium-Ion Battery Thermal Management System. *Chin. J. Mech. Eng. (Engl. Ed.)* **2022**, *35*, 100. [[CrossRef](#)]
89. Abdelkareem, M.A.; Maghrabie, H.M.; Abo-Khalil, A.G.; Adhari, O.H.K.; Sayed, E.T.; Radwan, A.; Elsaid, K.; Wilberforce, T.; Olabi, A.G. Battery Thermal Management Systems Based on Nanofluids for Electric Vehicles. *J. Energy Storage* **2022**, *50*, 104385. [[CrossRef](#)]
90. Khan, I.; Saeed, K.; Khan, I. Nanoparticles: Properties, Applications and Toxicities. *Arab. J. Chem.* **2019**, *12*, 908–931. [[CrossRef](#)]
91. Awais, M.; Ullah, N.; Ahmad, J.; Sikandar, F.; Ehsan, M.M.; Salehin, S.; Bhuiyan, A.A. Heat Transfer and Pressure Drop Performance of Nanofluid: A State-of-the-Art Review. *Int. J. Thermofluids* **2021**, *9*, 100065. [[CrossRef](#)]
92. Apmann, K.; Fulmer, R.; Soto, A.; Vafaei, S. Thermal Conductivity and Viscosity: Review and Optimization of Effects of Nanoparticles. *Materials* **2021**, *14*, 1291. [[CrossRef](#)] [[PubMed](#)]
93. Li, C.H.; Peterson, G.P. Mixing Effect on the Enhancement of the Effective Thermal Conductivity of Nanoparticle Suspensions (Nanofluids). *Int. J. Heat Mass Transf.* **2007**, *50*, 4668–4677. [[CrossRef](#)]
94. Al Shdaifat, M.Y.; Zulkifli, R.; Sopian, K.; Salih, A.A. Effect of CuO/Water Nanofluid as a Coolant for Liquid Cold Plate on Electric Vehicle Battery Cells. *Energy Sources Part A Recovery Util. Environ. Eff.* **2024**, *46*, 2270–2283. [[CrossRef](#)]
95. Thorat, P.; Sanap, S.; Gawade, S. A Comparative Study of Thermo-Physical Properties of Different Nanofluids for Effective Heat Transfer Leading to Li-Ion Battery Pack Cooling. *Energy Storage* **2024**, *6*, e566. [[CrossRef](#)]
96. Morali, U.; Yetik, O.; Karakoc, T.H. Nanofluid-Based Cooling of Prismatic Lithium-Ion Battery Packs: An Integrated Numerical and Statistical Approach. *J. Therm. Anal. Calorim.* **2024**, *149*, 799–811. [[CrossRef](#)]
97. Dhanasekaran, A.; Dhanasekaran, R.; Subramanian, Y.; Gubendiren, R.K.; Ali, M.; Raj, V.; Yassin, H.; Azad, A.K. Silver Nanofluid-Based Thermal Management for Effective Cooling of Batteries in Electric Vehicle Systems. *Arab. J. Sci. Eng.* **2024**, *49*, 14711–14728. [[CrossRef](#)]
98. Siddique, A.R.M.; Mahmud, S.; Heyst, B.V. A Comprehensive Review on a Passive (Phase Change Materials) and an Active (Thermoelectric Cooler) Battery Thermal Management System and Their Limitations. *J. Power Sources* **2018**, *401*, 224–237. [[CrossRef](#)]
99. Cui, X.; Jiang, S. A Novel Temperature Distribution Modeling Method for Thermoelectric Cooler with Application to Battery Thermal Management System. *Energy* **2024**, *306*, 132426. [[CrossRef](#)]

100. Cui, X.; Hu, T. Robust Predictive Thermal Management Strategy for Lithium-Ion Battery Based on Thermoelectric Cooler. *Appl. Therm. Eng.* **2023**, *221*, 119833. [[CrossRef](#)]
101. Lyu, Y.; Siddique, A.R.M.; Gadsden, S.A.; Mahmud, S. Experimental Investigation of Thermoelectric Cooling for a New Battery Pack Design in a Copper Holder. *Results Eng.* **2021**, *10*, 100214. [[CrossRef](#)]
102. Sait, H. Cooling a Plate Lithium-Ion Battery Using a Thermoelectric System and Evaluating the Geometrical Impact on the Performance of Heatsink Connected to the System. *J. Energy Storage* **2022**, *52*, 104692. [[CrossRef](#)]
103. Kharabati, S.; Saedodin, S. A Systematic Review of Thermal Management Techniques for Electric Vehicle Batteries. *J. Energy Storage* **2024**, *75*, 109586. [[CrossRef](#)]
104. Patel, J.R.; Rathod, M.K. Phase Change Material Selection Using Simulation-Oriented Optimization to Improve the Thermal Performance of Lithium-Ion Battery. *J. Energy Storage* **2022**, *49*, 103974. [[CrossRef](#)]
105. Verma, A.; Shashidhara, S.; Rakshit, D. A Comparative Study on Battery Thermal Management Using Phase Change Material (PCM). *Therm. Sci. Eng. Prog.* **2019**, *11*, 74–83. [[CrossRef](#)]
106. Huang, R.; Li, Z.; Hong, W.; Wu, Q.; Yu, X. Experimental and Numerical Study of PCM Thermophysical Parameters on Lithium-Ion Battery Thermal Management. *Energy Rep.* **2020**, *6*, 8–19. [[CrossRef](#)]
107. Rajan, J.T.; Jaypal, V.S.; Krishna, M.J.; Mohammed Firose, K.A.; Vaisakh, S.; John, A.K.; Suryan, A. Analysis of Battery Thermal Management System for Electric Vehicles Using 1-Tetradecanol Phase Change Material. *Sustain. Energy Technol. Assess.* **2022**, *51*, 101943. [[CrossRef](#)]
108. Chen, X.; Yang, H.K.; Song, Y.; Lai, W.; Zheng, L. Thermal Management System for Stable EV Battery Operation with Composite Phase Change Materials. *Phys. Scr.* **2024**, *99*, 6. [[CrossRef](#)]
109. El Idi, M.M.; Karkri, M.; Abdou Tankari, M. A Passive Thermal Management System of Li-Ion Batteries Using PCM Composites: Experimental and Numerical Investigations. *Int. J. Heat Mass Transf.* **2021**, *169*, 120894. [[CrossRef](#)]
110. Jilte, R.; Afzal, A.; Panchal, S. A Novel Battery Thermal Management System Using Nano-Enhanced Phase Change Materials. *Energy* **2021**, *219*, 119564. [[CrossRef](#)]
111. Behi, H.; Karimi, D.; Behi, M.; Narges, N.; Aminian, M.; Ghanbarpour, A.; Mirmohseni, F.; Van Mierlo, J.; Berecibar, M. An Enhanced Phase Change Material Composite for Electrical Vehicle Thermal Management. *Designs* **2022**, *6*, 70. [[CrossRef](#)]
112. Hussain, A.; Shahid, H.; Ali, I.; Ali, H.M. Passive Thermal Management System of Lithium-Ion Batteries Employing Metal Foam/PCM Composite for the Development of Electric Vehicles. *Energy Sources Part A Recovery Util. Environ. Eff.* **2023**, *45*, 505–522. [[CrossRef](#)]
113. Budiman, A.C.; Azzopardi, B.; Sudirja; Perdana, M.A.P.; Kaled, S.; Hadiastuti, F.S.; Hasyim, B.A.; Amin; Ristiana, R.; Muhamar, A.; et al. Phase Change Material Composite Battery Module for Thermal Protection of Electric Vehicles: An Experimental Observation. *Energies* **2023**, *16*, 3896. [[CrossRef](#)]
114. Nithin, V.K. A Comprehensive Review of Opportunities and Challenges in Heat Pipe Application: A Numerical Modeling. *J. Braz. Soc. Mech. Sci. Eng.* **2024**, *46*, 45. [[CrossRef](#)]
115. Weragoda, D.M.; Tian, G.; Burkitbayev, A.; Lo, K.H.; Zhang, T. A Comprehensive Review on Heat Pipe Based Battery Thermal Management Systems. *Appl. Therm. Eng.* **2023**, *224*, 120070. [[CrossRef](#)]
116. Brennan, P.J.; Krolczek, E.J. Heat Pipe Design Handbook. B & K Engineering, Inc.: Towson, MD, USA, 1979.
117. Abdelkareem, M.A.; Maghrabie, H.M.; Abo-Khalil, A.G.; Adhari, O.H.K.; Sayed, E.T.; Radwan, A.; Rezk, H.; Jouhara, H.; Olabi, A.G. Thermal Management Systems Based on Heat Pipes for Batteries in EVs/HEVs. *J. Energy Storage* **2022**, *51*, 104384. [[CrossRef](#)]
118. Behi, H.; Karimi, D.; Behi, M.; Jaguemont, J.; Ghanbarpour, M.; Behnia, M.; Berecibar, M.; Van Mierlo, J. Thermal Management Analysis Using Heat Pipe in the High Current Discharging of Lithium-Ion Battery in Electric Vehicles. *J. Energy Storage* **2020**, *32*, 101893. [[CrossRef](#)]
119. Vachhani, M.; Sagar, K.R.; Patel, V.M.; Mehta, H.B. Novel Integration of Dual Evaporator Loop Heat Pipe for Improved Electric Vehicle Battery Thermal Regulation. *Appl. Therm. Eng.* **2024**, *236*, 121832. [[CrossRef](#)]
120. Zheng, M.; Liu, Y.; Ma, Z.; Li, Y.; Li, D.; Lu, Z.; Song, H.; Guo, X.; Shao, W. Numerical Study on Power Battery Thermal Management System Based on Heat Pipe Technology. *Energy Rep.* **2023**, *9*, 350–361. [[CrossRef](#)]
121. Nasir, F.M.; Abdullah, M.Z.; Ismail, M.A. Effect of Heat Pipe's Configuration in Managing the Temperature of EV Battery. *CFD Lett.* **2023**, *15*, 22–34. [[CrossRef](#)]
122. Liu, H.; Ahmad, S.; Shi, Y.; Zhao, J. A Parametric Study of a Hybrid Battery Thermal Management System That Couples PCM/Copper Foam Composite with Helical Liquid Channel Cooling. *Energy* **2021**, *231*, 120869. [[CrossRef](#)]
123. Fan, Y.; Wang, Z.; Xiong, X.; Zhu, J.; Gao, Q.; Wang, H.; Wu, H. Novel Concept Design of Low Energy Hybrid Battery Thermal Management System Using PCM and Multistage Tesla Valve Liquid Cooling. *Appl. Therm. Eng.* **2023**, *220*, 119680. [[CrossRef](#)]
124. Hekmat, S.; Molaeimanesh, G.R. Hybrid Thermal Management of a Li-Ion Battery Module with Phase Change Material and Cooling Water Pipes: An Experimental Investigation. *Appl. Therm. Eng.* **2020**, *166*, 114759. [[CrossRef](#)]

125. Zhang, N.; Wang, Z.; Zhang, B.; Yang, H.; Bao, R.; Xiong, S.; Du, X.; Min, R. Performance Investigation of Battery Thermal Management System Based on L-Shaped Heat Pipe Coupled Cold Plate and Optimization of Controllable Liquid Cooling. *Eng. Appl. Comput. Fluid Mech.* **2024**, *18*, 2370941. [[CrossRef](#)]
126. Jang, D.S.; Yun, S.; Hong, S.H.; Cho, W.; Kim, Y. Performance Characteristics of a Novel Heat Pipe-Assisted Liquid Cooling System for the Thermal Management of Lithium-Ion Batteries. *Energy Convers. Manag.* **2022**, *251*, 115001. [[CrossRef](#)]
127. Cheng, J.; Shuai, S.; Zhao, R.; Tang, Z. Numerical Analysis of Heat-Pipe-Based Battery Thermal Management System for Prismatic Lithium-Ion Batteries. *J. Therm. Sci. Eng. Appl.* **2022**, *14*, 081008. [[CrossRef](#)]
128. Singh, L.K.; Kumar, R.; Gupta, A.K.; Sharma, A.K.; Panchal, S. Computational Study on Hybrid Air-PCM Cooling inside Lithium-Ion Battery Packs with Varying Number of Cells. *J. Energy Storage* **2023**, *67*, 107649. [[CrossRef](#)]
129. Chen, X.; Yang, W.; Shen, J.; Xu, X.; Zhou, F. Thermal Performance of Hybrid Battery Thermal Management System with Air Cooling and Phase Change Material Embedding Biomimetic Variable Section Fins. *Appl. Therm. Eng.* **2023**, *231*, 120985. [[CrossRef](#)]
130. Carbajal, G. Study of Different Flow Configurations and Heat Pipe Combination Effects in Air Cooling Systems. In Proceedings of the ASME 2022 International Mechanical Engineering Congress and Exposition, Columbus, OH, USA, 30 October–3 November 2022. V008T11A041.
131. Saechan, P.; Dhuchakallaya, I.; Al Zahrah Mohd Saat, F. Thermal Performance Improvement of Forced-Air Cooling System Combined with Liquid Spray for Densely Packed Batteries of Electric Vehicle. *Eng. Sci.* **2023**, *24*, 886. [[CrossRef](#)]
132. Al Tahhan, A.B.; AlKhedher, M.; Ramadan, M.; ElCheikh, A.; Choi, D.S.; Ghazal, M. Experimental and Numerical Analysis of a Liquid-Air Hybrid System for Advanced Battery Thermal Management. *Appl. Therm. Eng.* **2024**, *253*, 123754. [[CrossRef](#)]
133. Andersson, M.; Streb, M.; Ko, J.Y.; Löfqvist Klass, V.; Klett, M.; Ekström, H.; Johansson, M.; Lindbergh, G. Parametrization of Physics-Based Battery Models from Input–Output Data: A Review of Methodology and Current Research. *J. Power Sources* **2022**, *521*, 230859. [[CrossRef](#)]
134. Zou, L. Meta-Learning Basics and Background. In *Meta-Learning*; Elsevier: Amsterdam, The Netherlands, 2023; pp. 1–22.
135. Wang, Y.; Seo, B.; Wang, B.; Zamel, N.; Jiao, K.; Adroher, X.C. Fundamentals, Materials, and Machine Learning of Polymer Electrolyte Membrane Fuel Cell Technology. *Energy AI* **2020**, *1*, 100014. [[CrossRef](#)]
136. Smiti, A. When Machine Learning Meets Medical World: Current Status and Future Challenges. *Comput. Sci. Rev.* **2020**, *37*, 100280. [[CrossRef](#)]
137. Hasan, M.M.; Ali Pourmousavi, S.; Jahanbani Ardakani, A.; Saha, T.K. A Data-Driven Approach to Estimate Battery Cell Temperature Using a Nonlinear Autoregressive Exogenous Neural Network Model. *J. Energy Storage* **2020**, *32*, 101879. [[CrossRef](#)]
138. Quazi, M.M.; Jalilantabar, F.; Kumarasamy, S.; Ezazi, M. Future of Battery Thermal Management Systems (BTMS): Role of Advanced Technologies, Artificial Intelligence and Sustainability. *Next Sustain.* **2025**, *6*, 100114. [[CrossRef](#)]
139. Zhao, G.; Wang, X.; Negnevitsky, M.; Li, C. An Up-to-Date Review on the Design Improvement and Optimization of the Liquid-Cooling Battery Thermal Management System for Electric Vehicles. *Appl. Therm. Eng.* **2023**, *219*, 119626. [[CrossRef](#)]
140. Ghalkhani, M.; Habibi, S. Review of the Li-Ion Battery, Thermal Management, and AI-Based Battery Management System for EV Application. *Energies* **2023**, *16*, 185. [[CrossRef](#)]
141. Ghafoor, U.; Yaqub, M.W.; Qureshi, M.U.; Aslam Khan, M.N. Thermal Optimization of Li-Ion Battery Pack Using Genetic Algorithm Integrated with Machine Learning. *Therm. Sci. Eng. Prog.* **2023**, *44*, 102069. [[CrossRef](#)]
142. Qian, X.; Xuan, D.; Zhao, X.; Shi, Z. Heat Dissipation Optimization of Lithium-Ion Battery Pack Based on Neural Networks. *Appl. Therm. Eng.* **2019**, *162*, 114289. [[CrossRef](#)]
143. Xu, Y.; Zhao, J.; Chen, J.; Zhang, H.; Feng, Z.; Yuan, J. Performance Analyses on the Air Cooling Battery Thermal Management Based on Artificial Neural Networks. *Appl. Therm. Eng.* **2024**, *252*, 123567. [[CrossRef](#)]
144. Shi, Y.; Ahmad, S.; Liu, H.; Lau, K.T.; Zhao, J. Optimization of Air-Cooling Technology for LiFePO<sub>4</sub> Battery Pack Based on Deep Learning. *J. Power Sources* **2021**, *497*, 229894. [[CrossRef](#)]
145. Jin, L.; Xi, H. Multi-Objective Parameter Optimization of the Z-Type Air-Cooling System Based on Artificial Neural Network. *J. Energy Storage* **2024**, *86*, 111284. [[CrossRef](#)]
146. Liu, Z.; Kabirzadeh, P.; Wu, H.; Fu, W.; Qiu, H.; Miljkovic, N.; Li, Y.; Wang, P. Machine Learning Enhanced Control Co-Design Optimization of an Immersion Cooled Battery Thermal Management System. *J. Appl. Phys.* **2024**, *136*, 025001. [[CrossRef](#)]
147. Tang, X.; Guo, Q.; Li, M.; Wei, C.; Pan, Z.; Wang, Y. Performance Analysis on Liquid-Cooled Battery Thermal Management for Electric Vehicles Based on Machine Learning. *J. Power Sources* **2021**, *494*, 229727. [[CrossRef](#)]
148. Zhou, X.; Guo, W.; Shi, X.; She, C.; Zheng, Z.; Zhou, J.; Zhu, Y. Machine Learning Assisted Multi-Objective Design Optimization for Battery Thermal Management System. *Appl. Therm. Eng.* **2024**, *253*, 123826. [[CrossRef](#)]
149. Kanti, P.K.; Yang, E.S.J.; Wanatasanappan, V.V.; Sharma, P.; Said, N.M. Impact of Hybrid and Mono Nanofluids on the Cooling Performance of Lithium-Ion Batteries: Experimental and Machine Learning Insights. *J. Energy Storage* **2024**, *101*, 113613. [[CrossRef](#)]
150. Afzal, A.; Alahmadi, A.A.; Abdul Razak, R.K.; Alwetaishi, M.; Alzaed, A.N.; Shaik, S. Machine Learning Prediction and Study of Hotspots and Hotspots Location for Sustainable Battery Energy System. *Int. J. Energy Res.* **2022**, *46*, 21045–21065. [[CrossRef](#)]

151. Jalilianabar, F.; Mamat, R.; Kumarasamy, S. Prediction of Lithium-Ion Battery Temperature in Different Operating Conditions Equipped with Passive Battery Thermal Management System by Artificial Neural Networks. *Mater. Today Proc.* **2021**, *48*, 1796–1804. [[CrossRef](#)]
152. Najafi Khaboshan, H.; Jalilianabar, F.; Abdullah, A.A.; Panchal, S.; Azarinia, A. Parametric Investigation of Battery Thermal Management System with Phase Change Material, Metal Foam, and Fins; Utilizing CFD and ANN Models. *Appl. Therm. Eng.* **2024**, *247*, 123080. [[CrossRef](#)]
153. Arif, A.; Reddy, V.S.N.; Srividya, K.; Mallampalli, U.T. Utilizing Multilayer Perceptron for Machine Learning Diagnosis in Phase Change Material-Based Thermal Management Systems. *Heat Transf.* **2024**, *53*, 4922–4947. [[CrossRef](#)]
154. Anooj, G.V.S.; Marri, G.K.; Balaji, C. A Machine Learning Methodology for the Diagnosis of Phase Change Material-Based Thermal Management Systems. *Appl. Therm. Eng.* **2023**, *222*, 119864. [[CrossRef](#)]
155. Sui, Z.; Lin, H.; Sun, Q.; Dong, K.; Wu, W. Multi-Objective Optimization of Efficient Liquid Cooling-Based Battery Thermal Management System Using Hybrid Manifold Channels. *Appl. Energy* **2024**, *371*, 123766. [[CrossRef](#)]
156. Ye, L.; Li, C.; Wang, C.; Zheng, J.; Zhong, K.; Wu, T. A Multi-Objective Optimization Approach for Battery Thermal Management System Based on the Combination of BP Neural Network Prediction and NSGA-II Algorithm. *J. Energy Storage* **2024**, *99*, 113212. [[CrossRef](#)]
157. Guo, C.Y.; Muhieldeen, M.W.; Teng, K.H.; Ang, C.K.; Lim, W.H. A Novel Thermal Management System for Lithium-Ion Battery Modules Combining Indirect Liquid-Cooling with Forced Air-Cooling: Deep Learning Approach. *J. Energy Storage* **2024**, *94*, 112434. [[CrossRef](#)]
158. Yang, Y.; Wang, Z.; Ayed, H.; Alhoee, J. Incorporating Nickel Foam with Nano-Encapsulated Phase Change Material and Water Emulsion for Battery Thermal Management: Coupling CFD and Machine Learning. *Case Stud. Therm. Eng.* **2024**, *60*, 104672. [[CrossRef](#)]
159. Monika, K.; Punnoose, E.M.; Datta, S.P. Multi-Objective Optimization of Cooling Plate with Hexagonal Channel Design for Thermal Management of Li-Ion Battery Module. *Appl. Energy* **2024**, *368*, 123423. [[CrossRef](#)]
160. Zheng, A.; Gao, H.; Jia, X.; Cai, Y.; Yang, X.; Zhu, Q.; Jiang, H. Deep Learning-Assisted Design for Battery Liquid Cooling Plate with Bionic Leaf Structure Considering Non-Uniform Heat Generation. *Appl. Energy* **2024**, *373*, 123898. [[CrossRef](#)]
161. Yuan, L.; Li, W.; Deng, W.; Sun, W.; Huang, M.; Liu, Z. Cell Temperature Prediction in the Refrigerant Direct Cooling Thermal Management System Using Artificial Neural Network. *Appl. Therm. Eng.* **2024**, *254*, 123852. [[CrossRef](#)]
162. Li, W.; Wang, Y.; Yang, W.; Zhang, K. Design and Optimization of an Integrated Liquid Cooling Thermal Management System with a Diamond-Type Channel. *Therm. Sci. Eng. Prog.* **2024**, *47*, 102325. [[CrossRef](#)]
163. Al-Haddad, L.A.; Ibraheem, L.; EL-Seesy, A.I.; Jaber, A.A.; Al-Haddad, S.A.; Khosrozadeh, R. Thermal Heat Flux Distribution Prediction in an Electrical Vehicle Battery Cell Using Finite Element Analysis and Neural Network. *Green Energy Intell. Transp.* **2024**, *3*, 100155. [[CrossRef](#)]
164. Bacak, A. Investigation of Maximum Temperatures in Lithium-Ion Batteries by CFD and Machine Learning. *Proc. Inst. Mech. Eng. Part D J. Automob. Eng.* **2024**, *239*, 2461–2471. [[CrossRef](#)]
165. Sukkam, N.; Katongtung, T.; Suttakul, P.; Mona, Y.; Achariyaviriya, W.; Tippayawong, K.Y.; Tippayawong, N. Machine Learning Prediction of a Battery's Thermal-Related Health Factor in a Battery Electric Vehicle Using Real-World Driving Data. *Information* **2024**, *15*, 553. [[CrossRef](#)]
166. Jiang, Q.; Zhang, Y.; Liu, Y.; Xu, R.; Zhu, J.; Wang, J. Structural Optimization of Serpentine Channel Water-Cooled Plate for Lithium-Ion Battery Modules Based on Multi-Objective Bayesian Optimization Algorithm. *J. Energy Storage* **2024**, *91*, 112136. [[CrossRef](#)]
167. Li, W.; Wang, N.; Garg, A.; Gao, L. Multi-Objective Optimization of an Air Cooling Battery Thermal Management System Considering Battery Degradation and Parasitic Power Loss. *J. Energy Storage* **2023**, *58*, 106382. [[CrossRef](#)]
168. Zhang, F.; He, Y.; Wang, C.; Liang, B.; Zhu, Y.; Gou, H.; Xiao, K.; Lu, F. A New Type of Liquid-Cooled Channel Thermal Characteristics Analysis and Optimization Based on the Optimal Characteristics of 24 Types of Channels. *Int. J. Heat Mass Transf.* **2023**, *202*, 123734. [[CrossRef](#)]
169. Fan, Z.; Fu, Y.; Liang, H.; Gao, R.; Liu, S. A Module-Level Charging Optimization Method of Lithium-Ion Battery Considering Temperature Gradient Effect of Liquid Cooling and Charging Time. *Energy* **2023**, *265*, 126331. [[CrossRef](#)]
170. Fan, Y.; Wang, Z.; Xiong, X.; Panchal, S.; Fraser, R.; Fowler, M. Multi-Objective Optimization Design and Experimental Investigation for a Prismatic Lithium-Ion Battery Integrated with a Multi-Stage Tesla Valve-Based Cold Plate. *Processes* **2023**, *11*, 1618. [[CrossRef](#)]
171. Fan, Y.; Lyu, P.; Zhan, D.; Ouyang, K.; Tan, X.; Li, J. Surrogate Model-Based Multiobjective Design Optimization for Air-Cooled Battery Thermal Management Systems. *Eng. Appl. Comput. Fluid Mech.* **2022**, *16*, 1031–1047. [[CrossRef](#)]
172. Çolak, A.B. Comparative Investigation of the Usability of Different Machine Learning Algorithms in the Analysis of Battery Thermal Performances of Electric Vehicles. *Int. J. Energy Res.* **2022**, *46*, 21104–21126. [[CrossRef](#)]

173. Yalçın, S.; Panchal, S.; Herdem, M.S. A CNN-ABC Model for Estimation and Optimization of Heat Generation Rate and Voltage Distributions of Lithium-Ion Batteries for Electric Vehicles. *Int. J. Heat Mass Transf.* **2022**, *199*, 123486. [[CrossRef](#)]
174. Liao, X.; Ma, C.; Peng, X.; Li, Y.; Duan, L.; Garg, A.; Gao, L. A Framework of Optimal Design of Thermal Management System for Lithium-Ion Battery Pack Using Multi-Objectives Optimization. *J. Electrochem. Energy Convers. Storage* **2021**, *18*, 021005. [[CrossRef](#)]
175. Chen, S.; Bao, N.; Garg, A.; Peng, X.; Gao, L. A Fast Charging–Cooling Coupled Scheduling Method for a Liquid Cooling-Based Thermal Management System for Lithium-Ion Batteries. *Engineering* **2021**, *7*, 1165–1176. [[CrossRef](#)]
176. Deng, T.; Ran, Y.; Yin, Y.; Liu, P. Multi-Objective Optimization Design of Thermal Management System for Lithium-Ion Battery Pack Based on Non-Dominated Sorting Genetic Algorithm II. *Appl. Therm. Eng.* **2020**, *164*, 114394. [[CrossRef](#)]
177. Garg, A.; Ruhatiya, C.; Cui, X.; Peng, X.; Bhalerao, Y.; Gao, L. A Novel Approach for Enhancing Thermal Performance of Battery Modules Based on Finite Element Modeling and Predictive Modeling Mechanism. *J. Electrochem. Energy Convers. Storage* **2020**, *17*, 021103. [[CrossRef](#)]
178. Lei, N.; Zhang, H.; Li, R.; Yu, J.; Wang, H.; Wang, Z. Physics-Informed Data-Driven Modeling Approach for Commuting-Oriented Hybrid Powertrain Optimization. *Energy Convers. Manag.* **2024**, *299*, 117814. [[CrossRef](#)]
179. Amba, G.; Rao, P.; Karthik, S.; Student, V.G.; Saurav, G.V.S.; Student, G.; Swetha, A. Numerical and Machine Learning Approaches for Effective Thermal Management with Phase Change Materials. *Appl. Therm. Eng.* **2022**, *222*. [[CrossRef](#)]
180. Goud, V.M.; Satyanarayana, G.; Ramesh, J.; Pathanjali, G.A.; Ruben Sudhakar, D. An Experimental Investigation and Hybrid Neural Network Modelling of Thermal Management of Lithium-Ion Batteries Using a Non-Paraffinic Organic Phase Change Material, Myristyl Alcohol. *J. Energy Storage* **2023**, *72*, 108395. [[CrossRef](#)]
181. Boonma, K.; Mesgarpour, M.; NajmAbad, J.M.; Alizadeh, R.; Mahian, O.; Dalkılıç, A.S.; Ahn, H.S.; Wongwises, S. Prediction of Battery Thermal Behaviour in the Presence of a Constructal Theory-Based Heat Pipe (CBHP): A Multiphysics Model and Pattern-Based Machine Learning Approach. *J. Energy Storage* **2022**, *48*, 103963. [[CrossRef](#)]
182. Muthya Goud, V.; Raval, F.; Ruben Sudhakar, D. A Sustainable Biochar-Based Shape Stable Composite Phase Change Material for Thermal Management of a Lithium-Ion Battery System and Hybrid Neural Network Modeling for Heat Flow Prediction. *J. Energy Storage* **2022**, *56*, 106163.
183. Kolodziejczyk, F.; Mortazavi, B.; Rabczuk, T.; Zhuang, X. Machine Learning Assisted Multiscale Modeling of Composite Phase Change Materials for Li-Ion Batteries’ Thermal Management. *Int. J. Heat Mass Transf.* **2021**, *172*, 121199. [[CrossRef](#)]
184. Zhang, N.; Zhang, Z.; Li, J.; Cao, X. Performance Analysis and Prediction of Hybrid Battery Thermal Management System Integrating PCM with Air Cooling Based on Machine Learning Algorithm. *Appl. Therm. Eng.* **2024**, *257*, 124474. [[CrossRef](#)]
185. Fini, A.T.; Fattahi, A.; Musavi, S. Machine Learning Prediction and Multiobjective Optimization for Cooling Enhancement of a Plate Battery Using the Chaotic Water-Microencapsulated PCM Fluid Flows. *J. Taiwan Inst. Chem. Eng.* **2023**, *148*, 104680. [[CrossRef](#)]
186. Wang, D.; Ali, M.A.; Alizadeh, A.; Chaturvedi, R.; Ali, M.R.; Sohail, M. A Numerical Investigation of a Two-Phase Nanofluid Flow with Phase Change Materials in the Thermal Management of Lithium Batteries and Use of Machine Learning in the Optimization of the Horizontal and Vertical Distances between Batteries. *Case Stud. Therm. Eng.* **2023**, *41*, 102582. [[CrossRef](#)]
187. Xie, S.; Xu, C.; Li, W.; Kang, Y.; Feng, X.; Wu, W. Machine Learning Accelerated the Performance Analysis on PCM-Liquid Coupled Battery Thermal Management System. *J. Energy Storage* **2024**, *100*, 113479. [[CrossRef](#)]
188. Chen, S.; Zhang, G.; Qiao, D.; Wang, X.; Jiang, B.; Dai, H.; Zhu, J.; Wei, X. A Neural Network-Based Regression Study for a Hybrid Battery Thermal Management System under Fast Charging. *SAE Int. J. Electrified Veh.* **2022**, *11*, 189–202. [[CrossRef](#)]
189. Liu, J.; Tavakoli, F.; Sajadi, S.M.; Mahmoud, M.Z.; Heidarshenas, B.; Aybar, H. Numerical Evaluation and Artificial Neural Network Modeling of the Effect of Oval PCM Compartment Dimensions around a Triple Lithium-Ion Battery Pack despite Forced Airflow. *Eng. Anal. Bound. Elem.* **2022**, *142*, 71–92. [[CrossRef](#)]
190. Alqaed, S.; Mustafa, J.; Mohammad Sajadi, S.; Ali Hamdan Alajmi, S.; Saleh Alsnan, M.; Aybar, H. Enhancing Thermal Performance of Cylindrical Li-Ion Battery Packs: A 3D Simulation with Strategic Phase Change Material Integration and Airflow Control. *Arab. J. Chem.* **2024**, *17*, 105835. [[CrossRef](#)]
191. Yang, W.; Zhou, F.; Liu, Y.; Xu, S.; Chen, X. Thermal Performance of Honeycomb-like Battery Thermal Management System with Bionic Liquid Mini-Channel and Phase Change Materials for Cylindrical Lithium-Ion Battery. *Appl. Therm. Eng.* **2021**, *188*, 116649. [[CrossRef](#)]

**Disclaimer/Publisher’s Note:** The statements, opinions and data contained in all publications are solely those of the individual author(s) and contributor(s) and not of MDPI and/or the editor(s). MDPI and/or the editor(s) disclaim responsibility for any injury to people or property resulting from any ideas, methods, instructions or products referred to in the content.